Notchless defines a stage-specific requirement for ribosome biogenesis during lineage progression in adult skeletal myogenesis

Barbara Gayraud-Morel, Marie Le Bouteiller, Pierre-Henri Commere, Michel Cohen-Tannoudji, Shahragim Tajbakhsh

© 2018. Published by The Company of Biologists Ltd | Development (2018) 145, dev162636. doi:10.1242/dev.162636

STEM CELLS AND REGENERATION

RESEARCH ARTICLE

Notchless defines a stage-specific requirement for ribosome biogenesis during lineage progression in adult skeletal myogenesis

Barbara Gayraud-Morel[1,2], Marie Le Bouteiller[2,3], Pierre-Henri Commere[4], Michel Cohen-Tannoudji[2,3] and Shahragim Tajbakhsh[1,2,*]

ABSTRACT

Cell fate decisions occur through the action of multiple factors, including signalling molecules and transcription factors. Recently, the regulation of translation has emerged as an important step for modulating cellular function and fate, as exemplified by ribosomes that play distinct roles in regulating cell behaviour. Notchless (Nle) is a conserved nuclear protein that is involved in a crucial step in ribosome biogenesis, and is required for the maintenance of adult haematopoietic and intestinal stem/progenitor cells. Here, we show that activated skeletal muscle satellite cells in conditional *Nle* mutant mice are arrested in proliferation; however, deletion of *Nle* in myofibres does not impair myogenesis. Furthermore, conditional deletion of *Nle* in satellite cells during homeostasis did not impact on their fate for up to 3 months. In contrast, loss of Nle function in primary myogenic cells blocked proliferation because of major defects in ribosome formation. Taken together, we show that muscle stem cells undergo a stage-specific regulation of ribosome biogenesis, thereby underscoring the importance of differential modulation of mRNA translation for controlling cell fate decisions.

KEY WORDS: Ribosome biogenesis, Quiescence, Skeletal muscle stem cells, Regeneration, Notchless, Mouse

INTRODUCTION

In all cell types, protein synthesis is carried out by ribosomes, which are composed of proteins and RNA in two major subunits (Fromont-Racine et al., 2003; Peña et al., 2017). Although this process was thought to be highly conserved in all eukaryotic cells, recent studies have shown that regulation of protein synthesis is an important mitigator of cell fate control (Buszczak et al., 2014; Signer et al., 2014; Zhang et al., 2014). For example, in the haematopoietic system, modulation of the phosphorylation of the eukaryotic factors 4E-BP1 (also known as EIF4EBP1) and 4E-BP2 (EIF4EBP2), which inhibit the cap-dependent translation initiation factor EIF4E, is crucial for tissue homeostasis and cell fate control (Signer et al., 2016). The regulation of mRNA translation has also been reported to be essential to regulate the quiescent-to-activation states of skeletal muscle stem cells (Zismanov et al., 2016).

Recent studies have shown that the role of ribosomal proteins is not limited to generic protein synthesis factories, but can be implicated in active regulation of spatiotemporal protein expression (Lindstrom, 2009; Xue and Barna, 2012). In addition, heterogeneities in ribosome composition point to another level of translational control of protein synthesis. Several reports have indicated that rRNAs or ribosomal proteins in diverse organisms and tissues are under temporal or cell-type regulation for ribosome biogenesis (Zhou et al., 2015). For example, during anterior-posterior patterning of the embryo, RPL38-associated ribosomes have an affinity for translation of a subset of Hox mRNAs through a specific internal ribosome entry site sequence (Kondrashov et al., 2011; Xue et al., 2015).

In addition to these new regulatory roles for ribosomes, attention has focused on ribosomopathies, which are a collection of disorders that involve ribosomal proteins or ribosomal components. Surprisingly, several ribosomal protein mutations produce tissue-specific phenotypes, but not a broad deficiency and loss of all cells, as the highly conserved structure of ribosomes might suggest (Armistead and Triggs-Raine, 2014; Mills and Green, 2017). Among these pathologies, several impact on red blood cell formation, such as Diamond-Blackfan anaemia or 5q-Syndrome, whereas others result in craniofacial abnormalities or spleen defects (Ross and Zarbalis, 2014; Zhou et al., 2015).

Ribosome biogenesis is a highly regulated complex process involving ∼200 different proteins that act in the folding and processing of rRNAs, ribosome sub-unit assembly and nuclear export (Peña et al., 2017). Several quality control checkpoints are involved (Pechmann et al., 2013; Peña et al., 2017) and errors in this process can trigger cell growth arrest or apoptosis, through a mechanism referred to as the ribosomal stress pathway (Golomb et al., 2014; Pechmann et al., 2013). Notchless (Nle; Nle1) is a pro-ribosomal protein that participates in the assembly of the pre-60S ribosomal unit in nucleoli (de la Cruz et al., 2005). In yeast, its orthologue Rsa4 is involved in the last steps of pre-60S formation in nucleoli before its export to the cytoplasm. Nle orchestrates nuclear export with other partners (Nerurkar et al., 2015; Peña et al., 2017). The ATPase Rea1 (Mdn1) allows release of Rsa4 from the 80S subunit in a GTPase-dependent manner, which only then can bind export proteins, such as the Crm1 protein that will direct the large subunit to the cytoplasm (Baßler et al., 2014; Matsuo et al., 2014). Although the precise function of Nle in this last step remains unclear, it has been proposed to promote a conformation change that permits quality control to be passed before export (Matsuo et al., 2014). In all cases, *Rsa4* or *Nle* deficiency in yeast or mammals, respectively, is lethal (de la Cruz et al., 2005; Cormier et al., 2006).

[1]Stem Cells and Development, Department of Developmental & Stem Cell Biology, Institut Pasteur, 25 rue du Dr Roux, 75015 Paris, France. [2]CNRS UMR 3738, Institut Pasteur, 25 rue du Dr Roux, 75015 Paris, France. [3]Early Mammalian Development and Stem Cell Biology, Department of Developmental & Stem Cell Biology, Institut Pasteur, 25 rue du Dr Roux, 75015 Paris, France. [4]Plateforme de Cytometrie, Institut Pasteur, 25 rue du Dr Roux, 75015 Paris, France.

*Author for correspondence (shahragim.tajbakhsh@pasteur.fr)

S.T., 0000-0003-1809-7202

Received 18 December 2017; Accepted 2 October 2018

Development (2018) 145, dev162636. doi:10.1242/dev.162636

Conditional ablation of *Nle* in adult mouse haematopoietic stem cells (HSCs) results in their loss (Le Bouteiller et al., 2013) yet deletion of *Nle* in B lymphocytes showed that this regulator is not required for their maintenance. In another context, conditional ablation of *Nle* with an inducible *Villin-CreERT2* resulted in the loss of intestinal stem and progenitor cells (Stedman et al., 2015).

Skeletal muscle satellite (stem) cells are quiescent in adult mice and can be identified by several markers, including the paired/homeodomain transcription factor Pax7 (Relaix and Zammit, 2012; Rocheteau et al., 2012; Seale et al., 2000). Following muscle injury, the cells undergo lineage progression from quiescence to proliferation and generate myoblasts that will differentiate to form new myofibres. Each cell state can be identified by a combination of markers. A small proportion of satellite cells return to their niche and self-renew during the regeneration process. In homeostatic adult mouse muscle, the turnover of satellite cells can vary in different muscles, but is considered to be relatively low (Keefe et al., 2015; Pawlikowski et al., 2015). Studies involving the incorporation of radiolabelled elements have shown that ribosomal proteins turnover to a certain extent in proliferating and differentiating muscle cells, with a reduced accumulation of ribosomes in myofibres compared with myoblasts (Agrawal and Bowman, 1987; Jacobs et al., 1985). Although these studies showed some heterogeneity in ribosomal proteins between proliferating and differentiating cells, there were discrepancies concerning the turnover of ribosomal proteins during differentiation. The role of ribosome biogenesis during muscle stem cell quiescence and activation has not been addressed to date.

Using a specific Cre inducible mouse model, we evaluated the requirement of *Nle*-mediated ribosome biosynthesis in distinct cell states during lineage progression in quiescent, proliferating and differentiated myogenic cells. We show that, in contrast to the transit amplification phase of myoblast production, which is dependent on the formation of newly synthesised ribosomes in an *Nle*-dependent manner, quiescent and differentiated cells appear to be independent of *Nle*-mediated ribosome formation. These findings point to distinct regulatory functions for *Nle*-dependent ribosome biogenesis in different myogenic cell states, and reveal a hitherto unappreciated level of regulation that can contribute to heterogeneity in the skeletal muscle lineage.

RESULTS

Stage-specific expression of *Nle* and ribosomal markers during myogenic commitment

Fluorescent *in situ* hybridisation (FISH), with rRNA probes hybridising to nucleolar precursors (Fig. 1A), was used to quantify the levels of rRNA present within the nucleolus of individual cells. The detection of interspaced transcriptional sequences (its) present in long transient nucleolar rRNA species before being fully processed was used as a readout of ribosome biogenesis taking place in a given cell (its1 and its2 probes detect rRNA precursors of the small and large subunit, respectively). Freshly isolated single myofibres (T0 h) were used to evaluate ribosome biogenesis in quiescent satellite cells and myonuclei simultaneously. As all satellite cells express *Pax7* in homeostatic muscle, *Tg:Pax7-nGFP* mice (Sambasivan et al., 2009) were used to identify quiescent satellite cells located on the myofibre surface. Quantification of its1 and its2 FISH signals showed a significantly lower expression in quiescent satellite cells compared with the robust levels detected in all myonuclei (Fig. 1B,C). When myofibres are cultured in suspension, satellite cells activate to generate myoblasts (>80% divide within 24 h) and express the myogenic commitment gene *Myod* (*Myod1*) within 24 h (Rocheteau et al., 2012; Siegel et al., 2011; Zammit and Beauchamp, 2001). Quantification of FISH signals in the Pax7-nGFP^{+} cells at 48 h showed a marked increase of the its1 and its2 signals, reflecting the increased activity of ribosome biogenesis in these proliferating myogenic cells (Fig. 1D,E). This increase in rRNA precursor levels was also detected by RT-qPCR on quiescent and *in vitro* activated Pax7-nGFP^{+} cells that had been isolated by fluorescence-activated cell sorting (FACS) (Fig. 1F). Accordingly, the level of 18S and 28S rRNAs was high in activated satellite cells (Fig. S1A). These results show that the demand on ribosome biogenesis is low in satellite cells, as is expected owing to their quiescent state, then the demand significantly increased during proliferation and was sustained in differentiated myofibres.

Consistent with these dynamics, *Nle* expression was low in quiescent satellite cells, it then increased upon activation and decreased in differentiated myofibres (Fig. 1G). A time course of *in vitro* cultured primary cells showed an increase in *Nle* transcript and protein levels as early as 3 h after their isolation by FACS (Fig. 1G,H). This increase correlated with the disappearance of the Notch-effector gene *HeyL*, which is a marker of quiescent satellite cells (Fig. 1I) (Mourikis et al., 2012). Nle protein can be identified *in vitro* and *in vivo* in proliferating myogenic cells (Fig. 1H). In addition, antibody staining of cultured wild-type single myofibres (Fig. 1J) or cells cultured for 24 h (Fig. S1B) showed nucleolar staining for Nle protein within Myod^{+} activated satellite cells, in contrast to quiescent satellite cells that had no detectable protein by immunofluorescence (Fig. 1J, Fig. S1B). Therefore, dynamic expression of rRNAs and Nle occurs in quiescent and activated satellite cells, and in differentiated myonuclei.

Loss of cyclinE expression and cell cycle progression in *Nle*-deficient primary myoblasts

To address the functional consequence of *Nle* deficiency in myogenic cells, we used transgenic *Tg:Pax7-CRE^{ERT2}* mice that allow inducible *Cre*-mediated recombination in quiescent and activated satellite cells (Mourikis et al., 2012). Crosses with mice carrying the *Nle^{flox}* (Le Bouteiller et al., 2013) and *Nle^{null}* (Cormier et al., 2006) alleles led to the generation of *Nle$^{flox/null}$;Tg:Pax7-Cre^{ERT2};Tg:Pax7-nGFP* (*Nle* cKO) and *Nle$^{flox/+}$;Tg:Pax7-Cre^{ERT2};Tg:Pax7-nGFP* (Cont) mice (Fig. S2A). *Cre*-mediated deletion of *Nle* was induced in satellite cells by providing tamoxifen in food to mice for 2 weeks, followed by a single tamoxifen injection to increase the number of recombined cells. Genomic polymerase chain reaction (PCR) showed an efficient deletion of up to 95% of the *Nle* allele in quiescent satellite cells under this regime (Fig. S2B,C). Accordingly, immunofluorescence staining of cultured cells showed that ∼95% of satellite cells lacked nucleolar staining for Nle protein (Fig. S2D,E).

To examine the requirement for *Nle* in proliferating myogenic cells, *Nle* cKO satellite cells were isolated by FACS 2 weeks after the last tamoxifen injection and cultured in growth medium for 20 h or 44 h (Fig. 2A). Interestingly, these cells adhered to the culture plate, but they did not spread as control cells (Fig. 2B). Tibialis anterior (TA) muscles were then injured by injection of cardiotoxin (CTX; a peptide from snake venom that induces myofibre lysis; Hardy et al., 2016) and pulsed with 5-ethynyl-2′-deoxyuridine (EdU) for 4 h before FACS at 20 h post-injury (pi). *Nle* cKO cells were significantly compromised in their ability to uptake EdU compared with control cells (Fig. S3A). mRNA was extracted directly from Pax7-nGFP^{+} primary myogenic cells isolated using FACS at 20 h and 44 h pi. Quantitative real-time PCR (RT-qPCR) showed a decline in *HeyL* transcript levels in *Nle* cKO cells, which

Development (2018) 145, dev162636. doi:10.1242/dev.162636

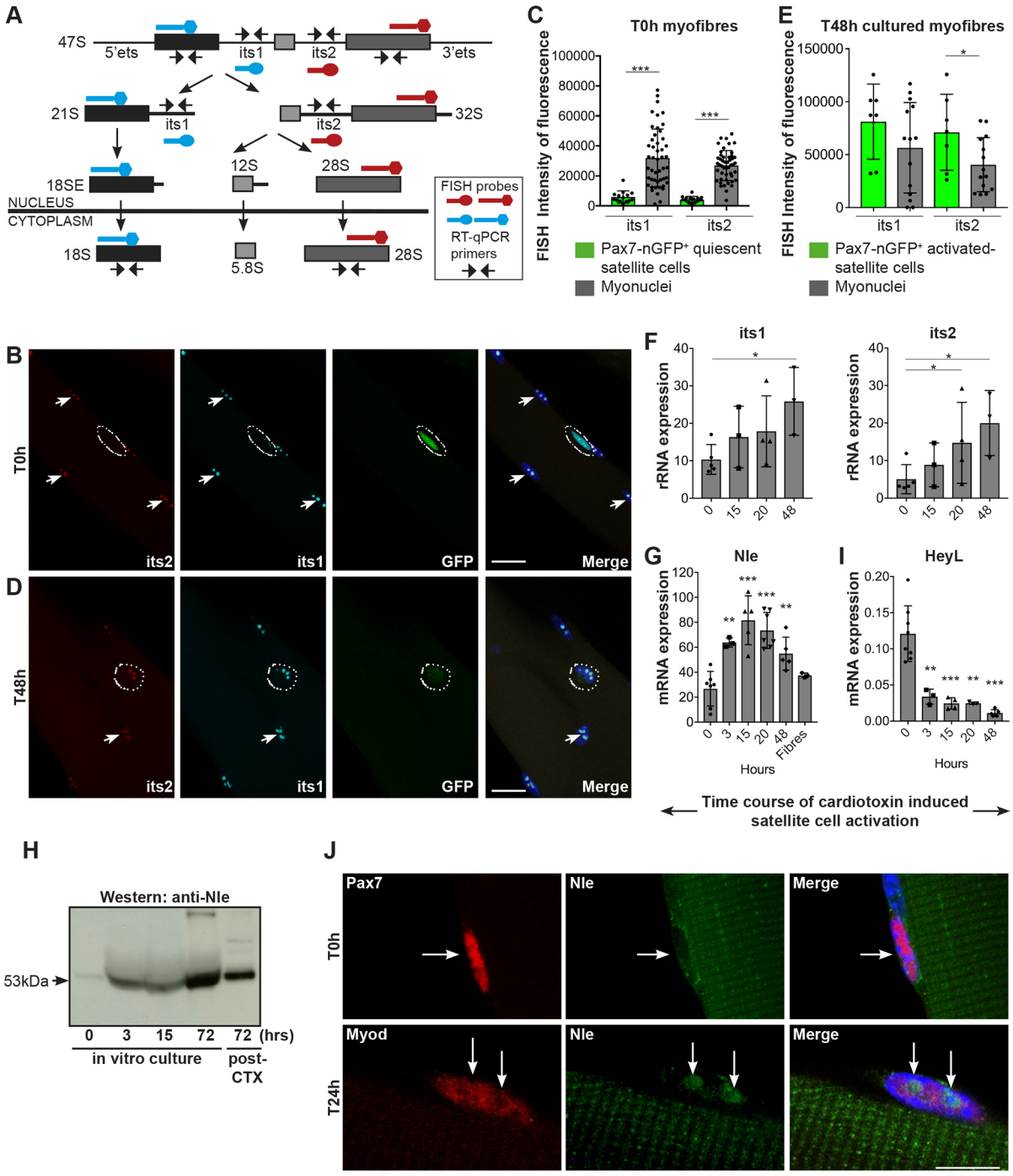

Fig. 1. See next page for legend.

indicates that they had exited quiescence as control cells (Mourikis et al., 2012); however, there was a marked loss of the cell cycle regulators cyclinE (Ccne1/Ccne2) and cyclinD1 (Ccnd1) (Fig. 2C, Fig. S3B).

Absence of transcripts and protein for the differentiation marker myogenin (Myog) indicated that the loss of proliferation was not a consequence of precocious differentiation (Fig. 2C; data not shown). In addition, after cell activation, *Myod* and *Myog* transcript levels were lower than in the control, whereas *Myf5* transcripts were unaffected (Fig. 2C, Fig. S3C). Clonal analysis of single cells cultured for 4 days and 3 weeks, as well as failure to uptake EdU *in vivo*, confirmed the compromised proliferative potential of *Nle* cKO cells (Fig. 2D, Fig. S3A). Genomic PCR confirmed the high recombination frequency in control cells and showed that rare large differentiated clones obtained from *Nle* cKO mice after 3 weeks in culture arose from non-deleted escaper cells (Fig. 2D, Fig. S3D).

As indicated above, the transition between the quiescent and proliferation state is associated with increased ribosome biogenesis and *Nle* expression (Fig. 1C,F). In the absence of *Nle*, we observed the accumulation of its2-containing rRNA precursors *in vivo* at 44 h after injury (Fig. 3A), consistent with a role for *Nle* in ribosomal large subunit maturation and export. Contrary to other cell types (Le Bouteiller et al., 2013; Stedman et al., 2015), *Nle* deficiency

Development (2018) 145, dev162636. doi:10.1242/dev.162636

Fig. 1. Stage specific expression of Nle and ribosomal markers during myogenic lineage progression. (A) Scheme of rRNA maturation. rRNA is initially transcribed in the nucleolus as a long 47S rRNA transcript, with external transcribed spacers at both ends (5′ets and 3′ets). This 47S rRNA is subjected to a series of cleavages to obtain the fully mature cytoplasmic 18S and 28S rRNA. Newly transcribed rRNA are detected in the nucleus by RT-qPCR primers or FISH probes directed against the intergenic sequences its1 and its2, which are present only in immature rRNA transcripts in nucleoli. Primers and FISH probes directed against the 18S and 28S sequences recognise both immature nucleolar and mature cytoplasmic rRNA transcripts. (B) Representative images of immature rRNA transcripts detected by FISH on freshly isolated (T0 h) *Tg:Pax7-nGFP* myofibres from EDL muscle. Nucleolar rRNA precursor transcripts were detected by FISH with probes recognising its1 and its2 sequences on quiescent satellite cells and myonuclei. Quiescent GFP$^+$ satellite cells (circled in white) show a low level of precursor rRNA, indicating low ribosome biogenesis compared with the higher levels in myonuclei (arrows). (C) Quantification of FISH signals on confocal images of freshly isolated myofibres (T0 h) (*n*=14 GFP$^+$ nuclei, *n*=40 myonuclei). (D) Representative images of FISH staining of immature rRNA transcripts in cultured (T24 h) *Tg:Pax7-nGFP* myofibres. The level of newly transcribed rRNAs detected with its1 and its2 probes increased greatly in the GFP$^+$ activated satellite cell (white circle) to a level comparable to that of myonuclei (arrows; *n*=14 GFP$^+$ nuclei, *n*=14 myonuclei). (E) Quantification of immunofluorescence intensity from FISH confocal microscopy images of isolated myofibres (T24 h). (F) Quantification by RT-qPCR of nucleolar rRNA using its1 and its2 detection. Time course for nucleolar rRNA shows an increase in 18S and 28S precursor rRNAs rapidly after injury-induced satellite cell activation. (G) Quantification by RT-qPCR of *Nle* expression in different cell states. Quiescent satellite cells were isolated by FACS from *Tg:Pax7-nGFP* limb muscles. Time course of activation was obtained from GFP$^+$ sorted cells from CTX-injured *Tg:Pax7-nGFP* TA muscles (3 h, 15 h, 20 h and 48 h after injury). Isolated EDL myofibres (fibres) represent the terminally differentiated muscle state. (H) Western blot for *Nle* expression on quiescent and activated satellite cells. GFP$^+$ satellite cells were isolated by FACS from *Tg:Pax7-nGFP* muscles at T0 h (quiescent) or *in vitro* activated for 3 h, 15 h, 72 h or 72 h after CTX-injury of TA muscle; 50,000 Pax7-nGFP$^+$ cells were loaded per lane. (I) Quantification by RT-qPCR of Notch-effector *HeyL* expression. (J) Nle nucleolar immunostaining in Pax7$^+$ quiescent (T0 h) or Myod$^+$ activated satellite cells (T24 h) in cultured wild-type EDL myofibres. Myofibre staining in the green channel corresponds to autofluorescence of skeletal muscle. *n*=3-8 mice for RT-qPCR for each time point. TBP was used as reference gene. Data represents mean±s.d. **P*<0.05; ***P*<0.005; ****P*<0.001 (two-tailed Student's *t*-test). In F,G,H, statistical significance is given compared with T0 h. Scale bars: 20 µm in B,D; 10 µm in J.

in satellite cells not only resulted in the accumulation of pre-60S rRNA precursors, but also a significant decrease in 28S rRNA transcript levels, and to some extent 18S rRNA transcripts, albeit the latter was not significant (Fig. 3A). FISH analysis of rRNA transcripts on plated satellite cells that were maintained for 24 h in culture showed a clear diminution of mature rRNA within the cytoplasm of the *Nle* cKO cells (Fig. 3B). Quantification of the intensity of fluorescence from FISH confocal images was performed on the nucleus and the cytoplasm for the 18S and 28S rRNAs. Measures of the surface area of the nuclear and cytoplasmic compartments highlight the failure of the *Nle* null cells to spread, activate and correctly increase nuclear and cytoplasmic volume compared with control cells (Fig. 3C). The reduction of ribosomal 18S and 28S rRNAs was observed mainly in the cytoplasm in *Nle* cKO cells (Fig. 3D).

Defective ribosome biogenesis is linked to the upregulation of the p53 (Trp53) signalling pathway, which leads to various cellular responses including cell cycle arrest and apoptosis (Golomb et al., 2014; Zhang et al., 2003). We used isolated single myofibres from control and cKO extensor digitorum longus (EDL) muscles to evaluate *p53* expression in quiescent and activated satellite cells. No p53 protein was detected in the quiescent cells (data not shown). After 24 h of culture, myofibre-associated satellite cells (GFP$^+$) were activated, as shown by the presence of Myod protein, and these cells lacked p53 protein (Fig. 3E,F). Strikingly, 80% of activated *Nle* cKO satellite cells expressed p53 protein at this stage (Fig. 3E,F). Collectively, our data show that, upon activation, *Nle*-deficient satellite cells display defective ribosomal large subunit production, which leads to a reduced quantity of cytoplasmic mature ribosomes and stabilisation of p53.

To confirm these observations, we examined satellite cells after their *in vivo* activation with CTX. Notably, the stabilisation of p53 corresponded to upregulation of several p53 target genes in *Nle* cKO cells, such as the cell cycle regulator p21 (Cdkn1a) and the pro-apoptotic genes *Bax* and *Noxa* (*Pmaip1*) (Fig. S4A,B). Apoptosis did not appear to be a major response to p53 stabilisation, as the proportion of *Nle* cKO satellite cells that were positive for activated caspase 3 was less than 2%, even after 72 h in culture (Fig. S4C). We then performed live videomicroscopy of cultured *Nle* cKO and control satellite cells to monitor their behaviour dynamically. In keeping with our findings, *Nle* cKO cells did not spread on the surface of the culture plate, they had limited motility, they did not undergo cell division and they displayed no significant cell death (Movie 1, Fig. S4D). In contrast, Cont cells were highly motile and performed multiple cell divisions during the same period (Movie 2, Fig. S4D). Nuclear and nucleolar staining performed either by FISH or immunostaining show distinct nucleoli and do not suggest a compromised integrity of this structure (Fig. 3B, Figs S4E,F).

We next investigated whether the defect in cell division was associated with reduced growth of cKO cells. We monitored the phosphorylation status of the S6-ribosomal protein RPS6, which is associated with cell growth and protein synthesis. In controls, phosphorylated (p)-RPS6 levels were low in quiescent satellite cells but increased after isolation and culture for 72 h (Fig. 3G,H,I). Although similar levels of p-RPS6 were noted in quiescent *Nle* cKO cells compared with the control, the mutant cells failed to upregulate p-RPS6 levels during this period, consistent with their compromised proliferation status. Accordingly, Myog protein was not detected in *Nle* cKO cells grown for 4 days in culture (Fig. S4F).

Conditional inactivation of *Nle* during adult muscle regeneration results in severe regeneration defects

The regeneration of *Nle* cKO TA muscle was evaluated by histology 8 days after CTX-induced injury. Newly regenerated myofibres with centrally located myonuclei, a hallmark of regenerated fibres, were observed throughout the control tissue sections (Fig. 4A). The density of mononucleated cells was increased in the mutant and necrotic myofibres persisted in some areas at 8 days pi (Fig. 4A). Quantification of regeneration showed that *Nle* cKO muscles had significantly fewer regenerated myofibres with centrally located myonuclei, which were reduced in cross-sectional area (Fig. 4B). Sirius Red staining on muscle sections showed that *Nle*-mutant TA muscles had higher levels of collagen deposition in the intercellular space, compared with the control (Fig. 4A). However, by 4 weeks pi histological analysis of the TA muscle showed that early regeneration defects were largely restored (Fig. 4C), with a number of myofibres almost equivalent to controls; however, these myofibres showed a smaller cross-sectional area compared with the control (Fig. 4D). Genomic PCR analysis on self-renewed Pax7-nGFP$^+$ cells isolated by FACS from 4 weeks pi TA muscle showed that these cells were not recombined for the *Nle^{flox}* allele and thus corresponded to escaper cells (Fig. 4E). Therefore, we propose that the rescued regeneration observed 4 weeks pi was due to escaper cells and that null cells do not contribute to muscle repair.

Development (2018) 145, dev162636. doi:10.1242/dev.162636

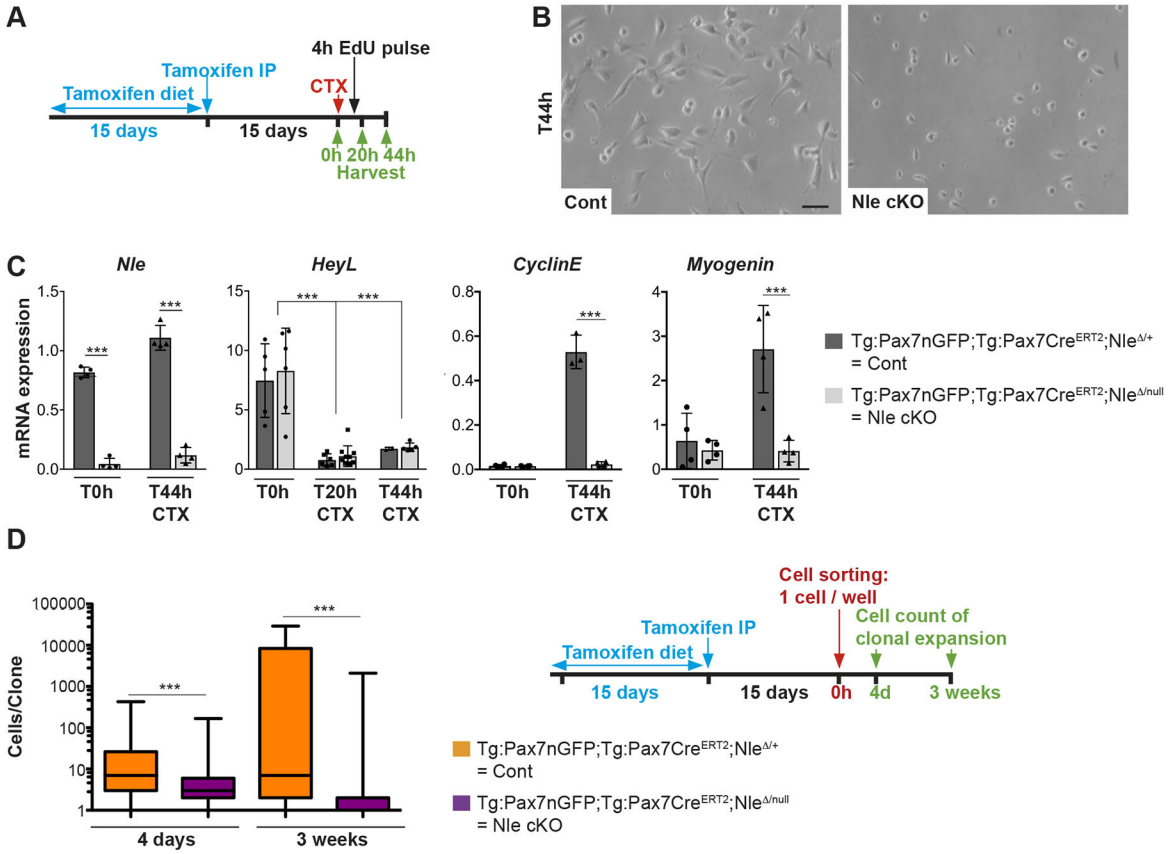

Fig. 2. Loss of cyclinE and cell cycle progression in *Nle* null primary myoblasts. (A) Scheme of tamoxifen-induction regime and cell harvest. GFP$^+$ satellite cells were isolated by FACS from hindlimb (quiescent) or TA muscles at 20 h or 44 h post-CTX injury (activated). Following the tamoxifen diet, animals generated were *Tg:Pax7-nGFP;Tg:Pax7Cre^{ERT2};Nle$^{\Delta/+}$* (Cont) and *Tg:Pax7-nGFP;Tg:Pax7Cre^{ERT2};Nle$^{\Delta/null}$* (*Nle* cKO). (B) Phase contrast microscopy of T44 h cultured cells showing that control cells spread and divided, but *Nle* cKO cells, which were plated at the same density, remained small and rounded in shape and rarely divided. (C) RT-qPCR quantification of transcripts expressed in Cont and *Nle* cKO cells. *Nle* transcripts were greatly reduced in quiescent and activated *Nle* cKO satellite cells. *HeyL* was downregulated in Cont and mutant CTX injury-induced activated satellite cells. Note, cyclinE induction failed in activated *Nle* cKO cells, and a reduction in *Myog* transcripts indicated reduced differentiation capacity; *n*=3-4 mice per time point; TBP was used as reference gene. (D) Clonal expansion at 4 days and 3 weeks post-plating following loss of *Nle*. Single GFP+ satellite cells were plated and the number of cells/colony was counted using Opera Phenix screening. At 4 days or 3 weeks, the mutant cells were unable to grow in culture and form colonies; *n*-values, opera experiment repeated 3 independent times with *n*=2 mice. Data represents mean±s.d. ***P<0.001 (two-tailed Student's *t*-test). Scale bar: 50 µm

Nle-mediated ribosome biogenesis acts in activated but not quiescent satellite cells

We then investigated whether *Nle* was required for the maintenance of quiescent satellite cells during homeostasis by quantifying the number of cells at different time points following tamoxifen injection. No change in the number of Pax7$^+$ cells was observed on freshly isolated EDL myofibres 9 days or 21 days post-tamoxifen treatment (Fig. 5A) or frozen sections of TA muscle stained for Pax7-nGFP$^+$ cells (Fig. S5A). The number of myofibres, and the number of myofibres with centrally located myonuclei, was not significantly altered between control and *Nle* mutant mice by 21 days (Fig. S5A). Given that satellite cells have a relatively low turnover (Chakkalakal et al., 2012; Keefe et al., 2015; Pawlikowski et al., 2015) we quantified, using FACS, the number of Pax7-nGFP$^+$ satellite cells at 12 weeks post-tamoxifen treatment in different muscles. No significant loss of satellite cells was observed between mutant and control TA, quadriceps and abdominal muscles (Fig. 5B). However, at 15 months post-tamoxifen treatment, a dramatic loss of satellite cells was observed in the *Nle* mutant TA, quadriceps and abdominal muscles (Fig. 5C) without a loss in muscle mass (Fig. S5B). Therefore, we propose that the spontaneous exit of satellite cells from quiescence over the 15 month period resulted in their loss, and that the satellite cell niche was not replenished. Genomic PCR on the remaining Pax7-nGFP$^+$ cells showed an absence of the deleted band and *Nle* mRNA expression was equivalent to the control (Fig. S5C), indicating that the remaining cells were not *Nle*-deleted and were likely cells that escaped the recombination process. Consistent with these results, a reduced number of centrally located myonuclei was observed in *Nle*-deficient TA muscles compared with 15-month-old control mice (Fig. S5D), suggesting that *Nle*-deleted satellite cells did not contribute to myofibres, whereas this occurs periodically in control mice during this period. Taken together, these findings suggest that, in the absence of *Nle*, satellite cells that spontaneously exit quiescence during homeostasis are not replenished by self-renewal of the pool over extended periods.

To investigate in more detail the phenotype of *Nle*-deficient quiescent satellite cells, we reasoned that the loss of *Nle* and ribosome biogenesis could affect their metabolic activity. Therefore, we quantified the mitochondrial content in satellite cells at 10 days (Fig. S5E) and up to 7 weeks post-tamoxifen treatment (Fig. 5D). Quantification of MitoTracker staining revealed no significant differences in mitochondrial content between *Nle* mutants and control quiescent cells (Fig. 5E, Fig. S5E). However, *in vitro* activated *Nle* cKO cells showed a 50% reduction in their mitochondrial content at 40 h after plating (Fig. 5F, Fig. S5E), and

Development (2018) 145, dev162636. doi:10.1242/dev.162636

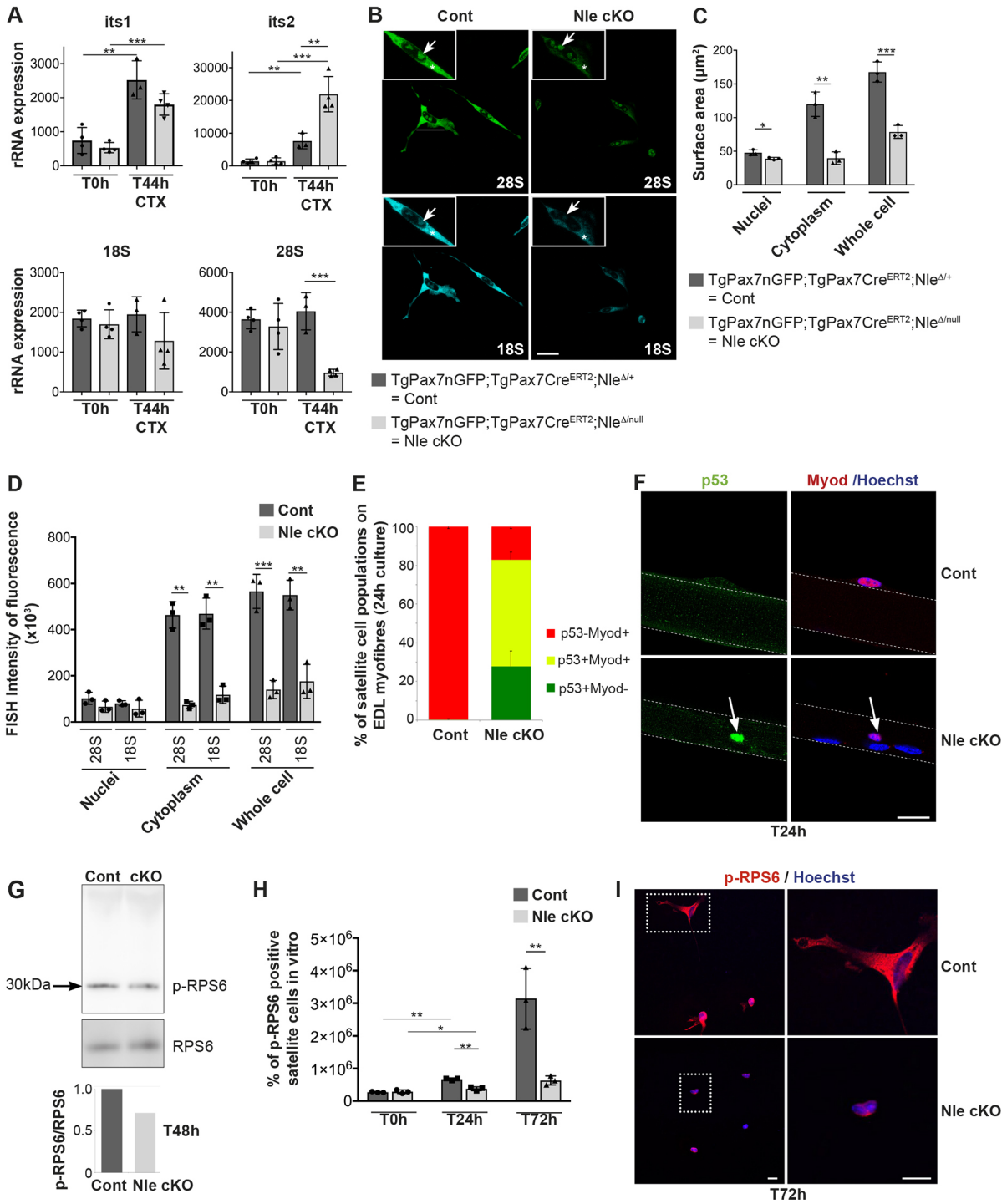

Fig. 3. Defective ribosome biogenesis in *Nle* mutant cells. (A) Quantification by RT-qPCR of nucleolar rRNA after *in vivo* satellite cell activation by CTX injury. After injury, the number of transcripts containing its2 nucleolar precursor rRNA increased in mutant cells, whereas the total number of 28S rRNA transcripts was markedly decreased, indicating a major defect in the synthesis of the large 60S subunit. After injury, *in vivo* activated satellite cells showed a minor decrease in the number of small 40S subunit rRNAs. (B) Representative images of FISH detection of nucleolar and cytoplasmic rRNA transcripts in cultured cells. FISH with the 18S and 28S probes shows a marked decrease in the cytoplasmic staining of the mutant cells after *in vitro* culture. Insets indicate a magnified cell with the nucleolar domain indicated by an arrow and the cytoplasmic domain indicated by an asterisk. (C) Surface area of nucleus, cytoplasm and whole mutant and control cells. (D) Quantification of immunofluorescence intensity from FISH confocal microscopy images of cells cultured for 24 h. *Nle* mutant cells show a marked decrease in their cytoplasmic rRNA content *in vitro* (n=3 mice). (E) p53 expression in quiescent and activated myofibre-associated satellite cells. After 24 h in culture, activated satellite cells expressed Myod, but only the *Nle* cKO cells upregulated p53 (n=2, Cont; n=4 *Nle* cKO, with 50-200 cells counted/mouse). (F) Immunostaining for p53 and Myod$^+$ on activated satellite cells from 24 h cultured EDL single myofibres. Arrows indicate activated satellite cell. Dotted lines indicate the myofibre membrane. (G) Western blot of p-RPS6 from 48 h cultured cells. Graph shows the relative quantification of the ratio p-RPS6/RPS6 band intensities. (H) Percentage of quiescent and activated satellite cells positive for p-RPS6. For each mouse, ~100 cells were quantified for p-RPS6 staining; n=3 mice. (I) Representative images of p-RPS6 immunostaining of Cont and *Nle* cKO cells after 72 h in culture. Boxed area in left panel is shown at a higher magnification in the right panel. n=3-4 mice for each time point for RT-qPCR. TBP was used as reference gene. Data represents mean±s.d. *P<0.05; **P<0.005; ***P<0.001 (two-tailed Student's t-test). Scale bars: 20 µm.

Development (2018) 145, dev162636. doi:10.1242/dev.162636

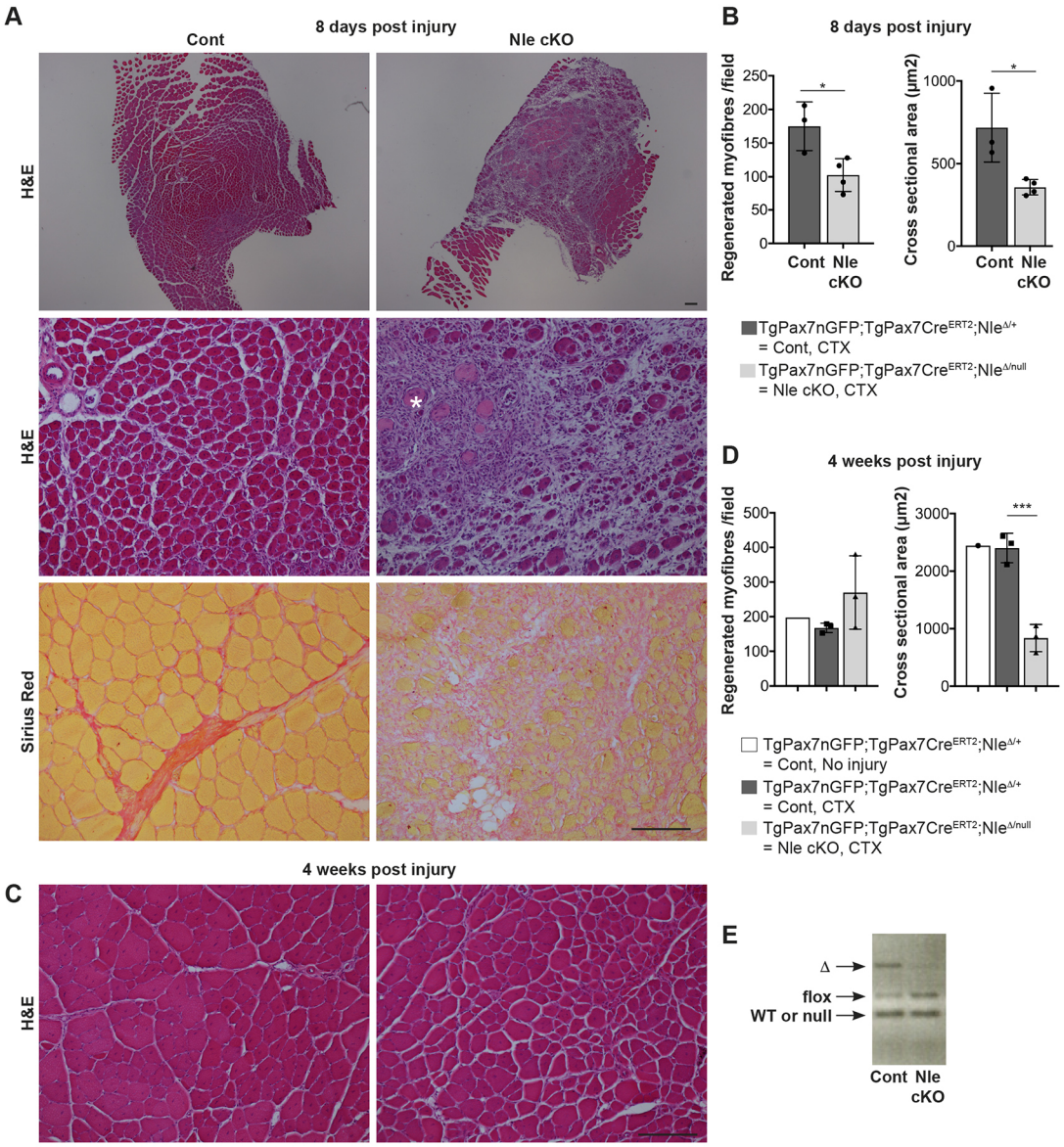

Fig. 4. Conditional ablation of *Nle* during adult muscle regeneration results in severe regeneration defects. (A) Haematoxylin and Eosin staining on Cont and *Nle* cKO TA sections 8 days after CTX injury. *Nle*-deficient TA muscle shows severe impairment in regeneration. High magnification shows sparse myofibres with centrally located myonuclei in mutant muscle, considerable infiltrating cells and necrotic fibres (asterisk), whereas control sections were homogeneously filled with regenerated myofibres. Sirius Red staining in Cont and mutant TA sections shows the increased collagen deposition in mutant injured muscles (collagen deposition in red). (B) Quantification and cross-sectional areas of regenerated myofibres with centrally located myonuclei. (C) Haematoxylin and Eosin staining on Cont and *Nle* cKO TA muscle sections 4 weeks after CTX injury. (D) Quantification and cross-sectional areas of regenerated myofibres with centrally located myonuclei 4 weeks pi. Mutant TA muscle shows a complete but impaired regeneration with a higher number of smaller myofibres. (E) Genomic PCR of self-renewed Pax7-nGFP^{+} cells isolated by FACS from 4 weeks pi of TA muscle (n=3 mice). Data represents mean±s.d. *P<0.05; ***P<0.001 (two-tailed Student's t-test). Scale bars: 100 µm

this reduction reached 80% when the distinction between *Nle*-deficient cells and escaper cells was taken into account (Fig. 5G, Fig. S5E). Indeed, genomic PCR analysis of the two populations (R6 and R7 populations) obtained by FACS of the 40 h activated *Nle* cKO cells clearly demonstrated that the more abundant population with the lower mitochondria content corresponded to *Nle*-deficient cells, whereas the minor population with the mitochondrial content similar to control cells corresponded to escaper cells (Fig. S5F).

Nle-mediated ribosome biogenesis is dispensable in differentiated myofibres

To assess the function of *Nle* in differentiated muscle cells, we used the transgenic alpha-skeletal actin-Cre (*Tg:HSA-Cre*) mouse to delete *Nle* specifically in differentiated myofibres (*HSA-Nle KO* mutants) throughout prenatal and postnatal development, but not in quiescent or proliferating myoblasts (Miniou et al., 1999). Recombination of the *Nle* flox allele (Nle^{Δ}) was readily observed by genomic PCR from whole abdominal muscle extracts (Fig. 6A). The efficient deletion of *Nle* in Cont and mutant differentiated muscle cells was also observed in 2-month-old EDL isolated myofibres (Fig. 6A). Consequently, *Nle* transcripts were absent in myofibres (Fig. 6B), but mRNA for the structural protein troponin was detectable (Fig. 6B). Although ribogenesis was sustained to a high level in differentiated myofibres (Fig. 1B,C), deletion of *Nle* from embryogenesis to adulthood resulted in no overt phenotype, as total body weight and TA muscle weight were similar between *HSA-Nle KO* mutants and controls (Fig. 6C).

Development (2018) 145, dev162636. doi:10.1242/dev.162636

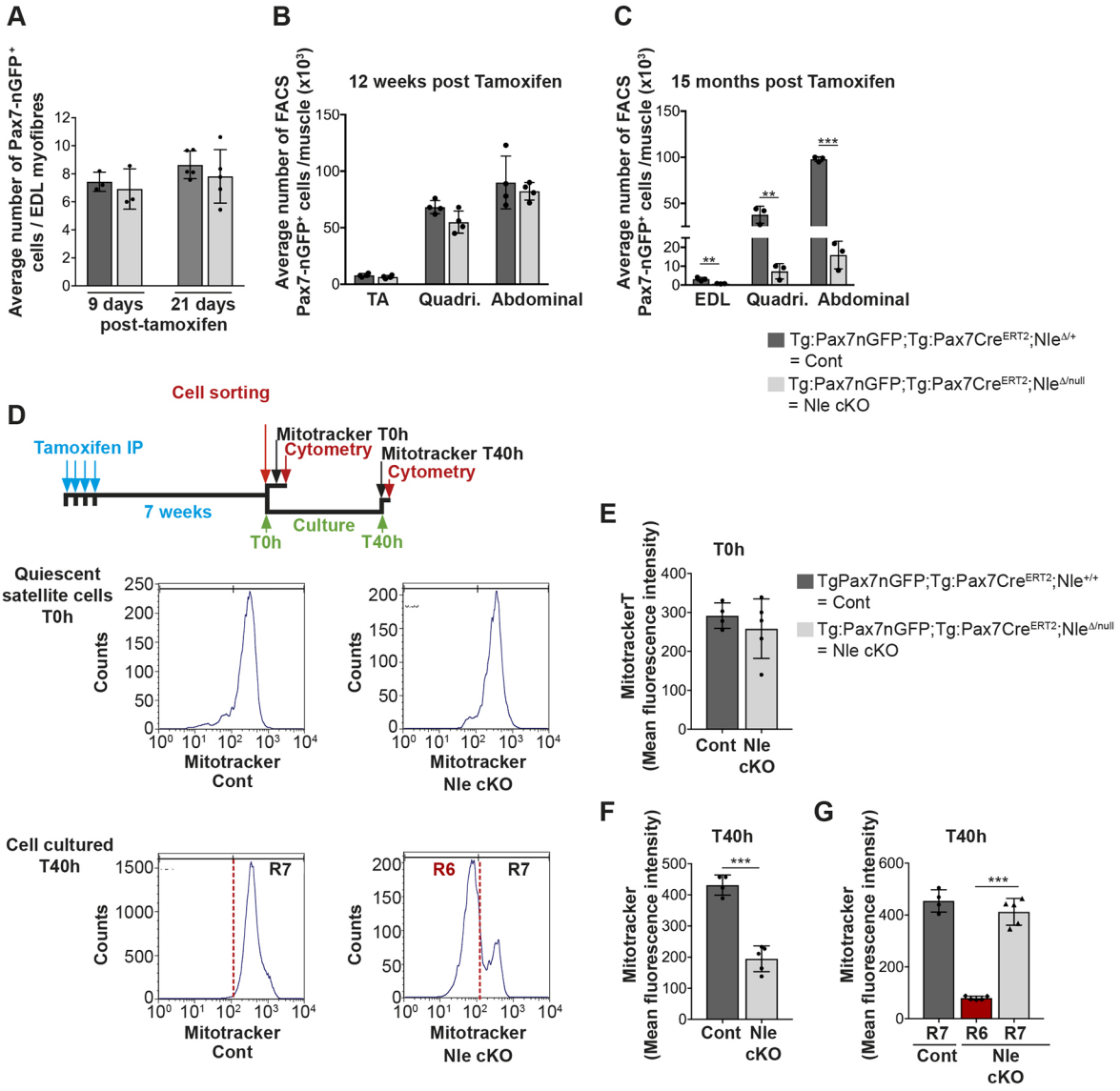

Fig. 5. *Nle*-mediated ribosome biogenesis acts in activated but not quiescent satellite cells. (A) Quantification of Pax7$^+$ cells on isolated EDL myofibres, 9 or 21 days after tamoxifen injections (n=3 mice). (B) Quantification of Pax7-nGFP$^+$ cells isolated from TA, quadriceps and abdominal muscles, up to 12 weeks after *Nle*-induced deletion by tamoxifen diet (n=5 mice). (C) Quantification of Pax7-nGFP$^+$ cells isolated by FACS from EDL, quadriceps and abdominal muscles, 15 months after *Nle*-induced deletion by tamoxifen diet (n=4 mice). (D) Top panel shows a schematic of MitoTracker treatment of cells isolated by FACS. Bottom panels indicate mitochondrial content in *Nle*-deficient cells. FACS profile of the mitochondrial content (x-axis, Deep Red MitoTracker) of Pax7-nGFP$^+$ *Nle* cKO and Cont cells immediately after cell sorting (quiescent) or 40 h after cell culture (activated). The red line in the lower panels marks the boundary between two cell populations observed in cKO cells. (E) Mean fluorescent intensity of MitoTracker labelling on quiescent *Nle* cKO and Cont cells (n=4 mice). (F) Mean fluorescent intensity of MitoTracker labelling on T40 h cell culture of *Nle* cKO and Cont cells (n=4-5 mice). (G) Mean fluorescent intensity of MitoTracker labelling in distinct R6 (red) and R7 cell populations observed in activated *Nle* cKO cells (see R6 and R7 cell populations labelled in panel D). The mitochondrial content analysis of the *Nle* mutation sample shows that the R7 fractions correspond to escaper cells, whereas R6 fractions correspond to *Nle*-deleted cells. Data represents mean±s.d. **P<0.005; ***P<0.001 (two-tailed Student's t-test).

Furthermore, the cross-sectional area of individual TA myofibres did not show significant differences even in 4-month-old *HSA-Nle KO* mutants compared with control animals (Fig. 6D). In addition, FISH and RT-qPCR analysis showed no differences in the expression and content of 18S and 28S rRNA between 4-month-old mutant and control muscles (Fig. 6E-G). Taken together, these findings indicate that *Nle* does not play a major role in differentiated muscle fibres.

DISCUSSION

The differential regulation of translation in distinct contexts provides another level of control for modulating cell fate choices. The commitment and differentiation decisions of mammalian skeletal muscle stem cells have been studied extensively, yet the specific role of ribosome biogenesis in translation control has only recently begun to be explored. Our study reveals that Nle, an important factor for the maturation of the large ribosomal subunit, is essential for the activation and proliferation of myogenic cells, but it appears to be dispensable for the maintenance of quiescent stem cells and the generation of differentiated myofibres.

First, our results show that its1 and its2, which correspond to non-transcribed spacer regions that are present only in unprocessed forms of pre-rRNAs, are present in quiescent satellites at greatly reduced levels compared with activated or differentiated myonuclei, indicative of a reduced production of new ribosomes. This suggests

Development (2018) 145, dev162636. doi:10.1242/dev.162636

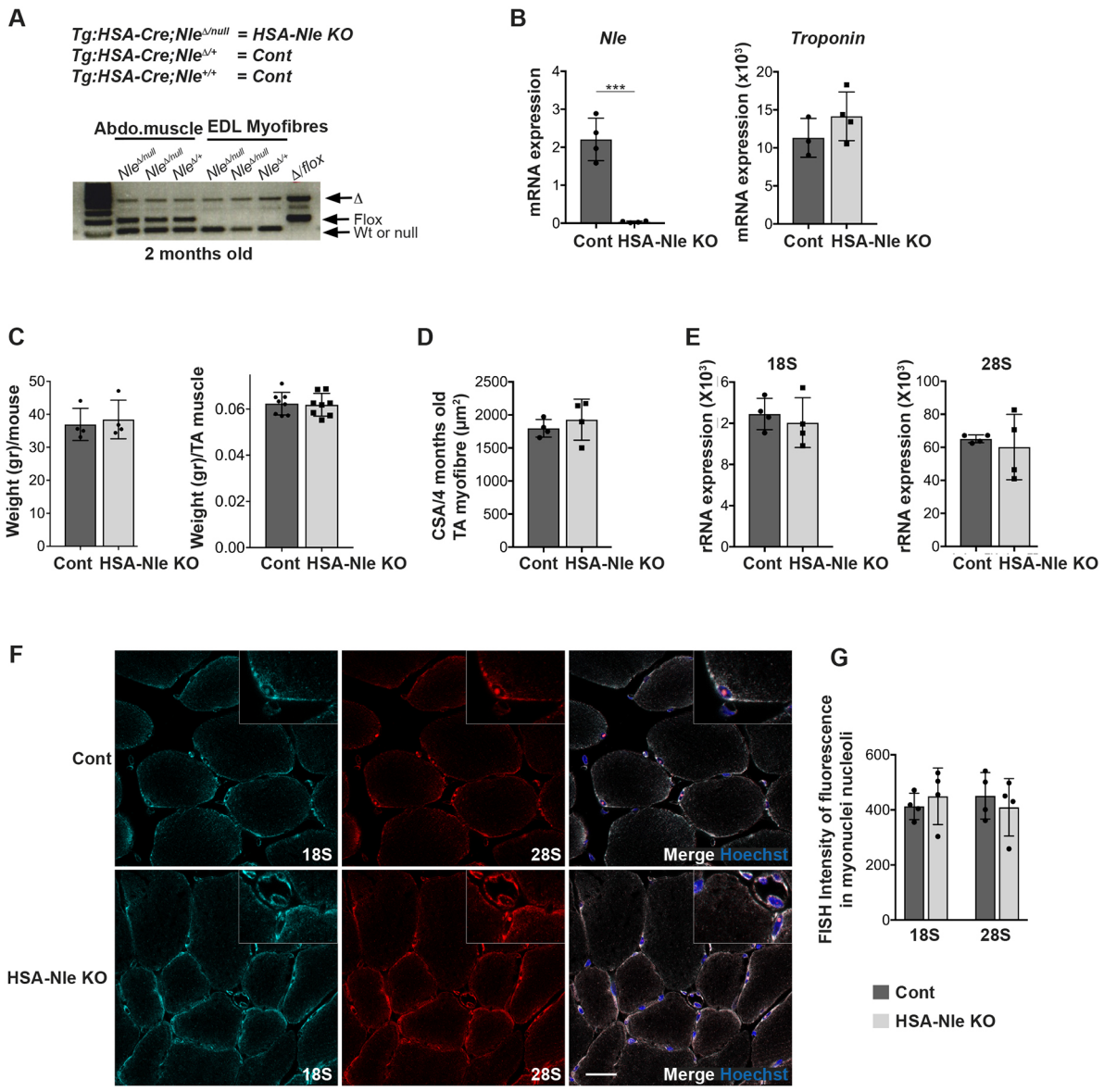

Fig. 6. Deletion of *Nle* in differentiated myofibres does not promote major deficits. (A) Genomic PCR for *Nle* deletion from *HSA-Nle KO* total abdominal muscle extract and 2-month-old isolated EDL myofibres. Genomic PCR from abdominal muscle, including differentiated muscle cells and non-muscle cells, shows the partial recombination of the *Nle* allele, whereas isolated myofibres containing only differentiated muscle cells show only the deleted *Nle* allele. (B) Quantification of *Nle* and troponin expression by RT-qPCR from myofibres. (C) Body weight of mice and TA muscle (n=4 mice). (D) Cross-sectional area of 4-month-old TA myofibres (n=4 mice). (E) Quantification of 18S and 28S rRNA transcripts by RT-qPCR from isolated EDL myofibres. (F) Representative confocal images of FISH experiments on TA muscle cryosections with rRNA 18S and 28S probes. Insets show magnification of myonuclei. (G) Quantification of immunofluorescence intensity from FISH confocal microscopy images of TA muscle cryosections that were hybridised with probes against 18S and 28S rRNA (n=4 mice). n=4 mice for RT-qPCR for each time point. TBP was used as reference gene. Data represents mean±s.d. ***P<0.001 (two-tailed Student's t-test). Scale bar: 25 µm.

that there is a low turnover of ribosomes. Similarly, decreased ribosome biogenesis was found in yeast that was forced to adopt a quiescent state following nutrient starvation (Gray et al., 2004). Maintenance of a low rate of protein synthesis in stem cells was also shown in quiescent and dividing HSCs through the control of the initiation factor 4E-BP1 (Buszczak et al., 2014; Signer et al., 2014). In quiescent satellite cells, phosphorylation of EIF2A has been reported to result in a general inhibition of mRNA translation, despite maintaining a high expression of some quiescent-specific mRNAs (Zismanov et al., 2016). However, in the nucleoli of *in vivo* and *in vitro* activated satellite cells and differentiated myonuclei, its1 and its2 are highly expressed, consistent with a higher demand for protein synthesis.

Furthermore, the demand for ribosome biogenesis to sustain protein synthesis in differentiated cells varies in different tissues. *In vitro* pulse-chase experiments with ^{14}C and ^{3}H radiolabelled amino acids in rat L6 (Jacobs et al., 1985) and MM14 mouse (Agrawal and Bowman, 1987) myoblasts and differentiated myofibres showed that the proportion of ribosomal proteins and rRNAs were reduced by half in the transition from proliferating myoblasts to differentiated myotubes in culture. How these findings correlate with *in vivo* myofibres that are subjected to constant muscle contractions is not clear. Our FISH analysis of its1 and its2 on freshly isolated myofibres provides some insights into *in vivo* rRNAs synthesis and ribosome formation. In humans, ribosome biogenesis has been coupled with hypertrophy following high

Development (2018) 145, dev162636. doi:10.1242/dev.162636

intensity training or the use of anabolic agents (Chaillou et al., 2014). Similarly, this inability to increase ribosome formation has been linked to the diminished capacity of aged muscle to hypertrophy (Stec et al., 2015). Interestingly, during denervation-induced atrophy, the ubiquitin and autophagy pathways are upregulated, leading to a loss of muscle mass, but the proteomic analysis revealed that ribosomal components were concomitantly upregulated (Lang et al., 2017). In future studies, it would be interesting to use proteomic approaches to examine ribosome turnover in these different cell states.

Ribosome assembly is a multistep process comprising hundreds of proteins, some of which are thought to be involved in mRNA translational control in a spatiotemporal manner. Perturbations in this process can result in tissue-specific defects (Kondrashov et al., 2011). Among these, Nle participates in the formation of the large 60S subunit and has specific roles in proliferating and differentiating cells (Le Bouteiller et al., 2013; Stedman et al., 2015). Here, we show that *Nle* expression is rapidly upregulated at the transcriptional and protein level, during the quiescence-to-activation transition of satellite cells following muscle damage. Loss of function of Nle showed that active Notch signalling declines as expected during this transition, an indication that Nle is not required for exit from the quiescent state. However, these cells fail to transit through S-phase, as shown by their inability to increase their cell size, express cyclinE, incorporate EdU and restore myofibres following muscle damage. In addition, *Myf5* transcription that is normally upregulated during the activation of satellite cells (Gayraud-Morel et al., 2012) remained unchanged in the *Nle* mutant cells. Although a requirement for Nle during the myogenic cell expansion was expected, the lack of phenotype in *Nle*-deficient myofibres was surprising. Both of these cell states require a sustained demand for protein synthesis. In skeletal muscle, the turnover of myofibrillar proteins is constant and is significantly increased upon physical activity, whereas it is maintained at a low level in resting muscle (Norton and Layman, 2006). Accordingly, we showed the presence of a high level of nucleolar rRNAs in myoblasts and differentiated myofibres, suggesting constant ribosome biogenesis. These results suggest that, as in HSCs (Le Bouteiller et al., 2013), *Nle* is dispensable for ribosome formation in differentiated myogenic cells. Studies in yeast have shown that the *Nle* homolog is crucial for nuclear export of the pre-60S subunit following its release by Rix-Rea1 (Peña et al., 2017). Therefore, our studies indicate that an Nle-independent mechanism acts in quiescent cells and differentiated myofibres for export of this ribosomal subunit.

Moreover, the absence of *Nle* normally triggers a p53-dependent ribosomal stress pathway in which impairment of ribosome formation promotes ribosomal proteins to bind to MDM2 and block MDM2-mediated p53 degradation, thereby inducing p53-dependent cellular responses including apoptosis and cell cycle arrest (Golomb et al., 2014; Zhang et al., 2003). During the quiescence-to-activation transition, p53 was detected in the majority of *Nle* null satellite cells, but not in control cells, consistent with the notion that ribosome biogenesis is disrupted during exit from quiescence in the absence of *Nle*. However, this upregulation of p53 did not correlate with the induction of apoptosis, but instead with a disruption of cell growth, as shown by the reduction of the phosphorylated form of RPS6. Taken together, these findings show that *Nle* plays stage-specific roles during lineage progression of satellite cells, as has been reported in highly proliferative tissues such as blood and intestine (Le Bouteiller et al., 2013; Stedman et al., 2015). However, in contrast to quiescent HSCs, *Nle* is dispensable for quiescent satellite cells.

Another unexpected observation from our results was the finding that the 28S rRNA was lost during the transition from quiescence to activation, a phenotype that was not observed previously for blood and intestine (Le Bouteiller et al., 2013; Stedman et al., 2015). This may be because of our ability to examine this transition with somewhat greater precision in muscle; however it remains unclear whether some 28S rRNA are degraded during this transition. The observed diminution of the 18S might be a consequence of the downregulation of 28S, as Nle is known to be mainly involved in large subunit formation. These observations raise the possibility that the transition state is dynamic for rRNA turnover and might reflect a previously unappreciated regulatory step.

In summary, our findings point to ribosome biogenesis, and specifically *Nle*, as crucial regulators of cell state transitions in skeletal muscle. Remarkably, the functional role of Nle is restricted to the proliferation state, but not the quiescent and differentiated states during lineage progression. These observations provide a framework for further investigations into the role of specific regulators of ribosome biogenesis in different physiological states.

MATERIALS AND METHODS

Mice and tamoxifen and EdU delivery

Nle deletion was obtained by crossing $Nle^{flox/+}$ and $Nle^{flox/null}$ mice (Cormier et al., 2006) to $Tg:Pax7\text{-}Cre^{ERT2}$ (Mourikis et al., 2012). In addition, the mice were crossed to transgenic *Tg:Pax7-nGFP* mice that allow the specific detection of the satellite cell population (Sambasivan et al., 2009). As a result, *Nle* cKO and Cont mice correspond to the following genotypes: $Tg:Pax7nGFP;Tg:Pax7Cre^{ERT2};Nle^{flox/null}$ and $Tg:Pax7nGFP;Tg:Pax7Cre^{ERT2};Nle^{flox/+}$, respectively. Unless specified, mice were fed with tamoxifen-granules (Harlan Laboratories) for 2 weeks and received tamoxifen by intraperitoneal (IP) injection (20 mg/ml tamoxifen solution diluted in corn oil) on the 15th day. After tamoxifen induction, the genotypes of mutant and control mice were: $Tg:Pax7nGFP;Tg:Pax7Cre^{ERT2};Nle^{\Delta/null}$ and $Tg:Pax7nGFP;Tg:Pax7Cre^{ERT2};Nle^{\Delta/+}$, respectively. *Nle* deletion in differentiated myofibres was carried out by crossing $Nle^{flox/+}$ and $Nle^{flox/null}$ mice to transgenic *Tg:HSA-Cre* mice (Miniou et al., 1999). The genotype of control and mutant mice were: $Tg:HSA\text{-}Cre;Nle^{\Delta/+}$ and $Tg:HSA\text{-}Cre;Nle^{\Delta/null}$. For proliferation experiments, mice were injected with EdU (Invitrogen) 4 h before sacrifice. Tails or cells were lysed overnight at 56°C in lysis buffer. Primers and strategy for genotyping by PCR have previously been described (Le Bouteiller et al., 2013). Animals were handled according to European Community guidelines and the ethics committee of the Institut Pasteur (CETEA) approved protocols.

Real-time RT-qPCR

Total RNA was extracted with RLT buffer (Qiagen RNeasy Micro Kit) or Tri Reagent (Sigma-Aldrich) for isolated single myofibres. cDNAs were prepared using reverse transcription (Super Script III, 18080044, Invitrogen) and real-time PCR was performed using SYBRGreen Universal Mix (13608700, Roche) or Taqman (04673417, Roche). Primers are listed in Table S1. Data were analysed using StepOnePlus RT PCR software v2.1 (Thermo Fisher Scientific) and Microsoft Excel. TBP transcript levels were used for normalisation of each target ($=\Delta C_T$). RT-qPCR C_T values were analysed using the $2^{-(\Delta\Delta CT)}$ method to calculate the fold expression (Livak and Schmittgen, 2001).

Immunostaining and histology

For indirect immunofluorescence, cells were plated and grown using the Permanox Nunc LabTek Chamber Slide System (177445, Thermo Scientific). Cells were then fixed with 4% paraformaldehyde (PFA; Electron Microscopy Sciences) for 5 min at room temperature (RT), rinsed 3× with PBS, permeabilised with 0.5% Triton X-100 for 10 min at RT and blocked for 20 min with 20% goat serum (Gibco) at RT. Primary antibodies were incubated overnight at 4°C, washed 3× with PBS and incubated for 2 h with Alexa-conjugated secondary antibody and Hoechst,

Development (2018) 145, dev162636. doi:10.1242/dev.162636

then washed 3× with PBS. Slides were mounted in PBS/80% glycerol before observation. Single myofibre preparations have been described (Gayraud-Morel et al., 2007). For detection of nascent RNA, 1 mM of 5-ethynyl uridine (Invitrogen) was added to the growth medium for 4 h before fixation and detection with Click-iT Reaction Kit (Invitrogen). Samples were observed using an inverted Observer microscope (Zeiss) or an SP5 confocal microscope (Leica). For histology, TA muscles were snap-frozen in liquid nitrogen-cooled-isopentane for 1 min and stored at −80°C before cryosectioning. For histology, cryosections (12 µm) were rinsed with PBS and fixed in 10% formalin for 3 min before staining with Haematoxylin and Eosin or with Sirius Red.

Isolation of satellite cells and cell culture

Quiescent and activated satellite cells were isolated from total limb muscles or injured TA muscles, respectively (Gayraud-Morel et al., 2017). Briefly, dissected muscles were collected into cold Dulbecco's Modified Eagle Medium (DMEM), minced with fine scissors and transferred into a 50 ml Falcon tube containing 20 ml of DMEM, 0.1% collagenase D (1088866, Roche), 0.25% trypsin (15090-046, Gibco), 0.1% DNAse1 10 mg/ml (11284932001, Roche) solution. The tube was gently agitated in a 37°C water bath for 30 min and kept standing without agitation for the last 5 min to allow muscle fragments to sediment. The supernatant was collected in a 50 ml Falcon tube containing 10% foetal bovine serum (FBS; Gibco) and kept on ice. A total of four rounds of digestion were required to dissociate the tissue. The supernatants were successively filtered through a 100 µm and a 70 µm cell strainer (Miltenyi Biotec), before being pooled and centrifuged at 4°C at 50 ***g*** for 10 min to clear larger debris (this step was omitted for satellite cell preparation from injured muscles). The pellet was discarded and the supernatant was then centrifuged at 500 ***g*** for 15 min to pellet the satellite cells. The supernatant was discarded and the pellet washed twice with 40 ml of cold DMEM. Before the last centrifugation, the cell suspension was filtered through a 40 µm cell strainer. The final pellet was suspended in 1 ml of DMEM/2% FBS, before cell sorting using a MoFlow Legacy FACS (Beckman Coulter Life Sciences). Sorted cells were collected in DMEM/20% FBS/Penicillin-Streptomycin or directly into Buffer RLT (Qiagen) for RNA extraction.

For cell culture, satellite cells were plated on 1 mg/ml Matrigel- (354234, Corning) coated dishes and grown in DMEM/F12 (Gibco) containing 20% FBS, 2% Ultroser-G (15950-017, Pall Biosepra) and Penicillin-Streptomycin (Gibco). For clonal analysis, a single Pax7-nGFP cell was distributed per well, using MoFlow Legacy FACS, on Matrigel-coated 96-well plates containing growth medium. Cells were maintained on growth medium for a period of 4 days or 3 weeks. Before cell analysis, the cells were fixed with 2% PFA and rinsed with PBS. Counting of cells/well was performed using the OPERA system.

FISH analysis

Fixed muscles that had been prepared for immunohistochemistry were sectioned and used for FISH staining. Plated cells or myofibres were fixed for 30 min with 4% PFA, rinsed with PBS and placed in 70% ethanol. Samples were rehydrated with 2× saline-sodium citrate buffer containing 10% formamide and processed as previously described (O'Donohue et al., 2010). Fluorochrome-conjugated probes (Eurogentec) are as follows: cy5-its1, 5′-TAGACACGGAAGAGCCGGACGGGAAAGA-3′; cy3-its2, 5′-GCGATTGATCGTCAACCGACGCTC-3′; cy5-18S, 5′-TTTACTTCC-TCTAGATAGTCAAGTTCGACC-3′; cy3- or Alexa 488-28S, 5′-CCCGT-TCCCTTGGCTGTGGTTTCGCTGGATA-3′; cy3-5′ets, 5′-AGAGAAAA-GAGCGGAGGTTCGGGACTCCAA-3′.

Mitochondrial staining

Cells that had been freshly isolated by FACS directly in DMEM without serum, or cells that had been cultured *in vitro*, were incubated in 200 nM Deep Red MitoTracker staining solution for 30 min at 37°C, washed with PBS and fixed in 2% PFA for 5 min at RT before analysis by sorting on a MoFlow Legacy cell sorter.

Western blot

Quiescent and injury-activated sorted satellite cells or *in vitro* cultured cells were collected in DMEM and counted with a Malassez cell counter; 50,000 cells for each condition were centrifuged and resuspended in radioimmunoprecipitation assay buffer plus protease inhibitors (Sigma-Aldrich). Cell lysates were run on 10% or 4-12% pre-casted gels (Novex). The gel was blotted onto a polyvinylidene difluoride membrane for 2 h at 200 mA at 4°C, and then saturated with 10% fat-free milk in Tris-buffered saline for 30 min at 4°C. The membrane was incubated with primary anti-Nle antibody (1:500) overnight at 4°C and with a secondary anti-rabbit HRP antibody (1:10,000) for 2 h (31460, Thermo Scientific Pierce Antibodies), then signal was revealed by Ecl-Plus (Pierce).

Antibodies

Primary antibodies used included: anti-GFP (chicken polyclonal, Abcam, ab13970, 1:1000), anti-laminin (rabbit polyclonal, Sigma-Aldrich, L-9393, 1:400), anti-Nle (rabbit polyclonal, 1:100, Le Bouteiller et al., 2013), anti-myogenin (mouse monoclonal, Developmental Studies Hybridoma Bank, F5D, 1:50), anti-Pax7 (mouse monoclonal, Developmental Studies Hybridoma Bank, Pax7, 1:50), anti-Myod (mouse monoclonal, Dako, Clone 5.8A, M3512, 1:100), anti-phospho-S6 ribosomal protein (rabbit polyclonal, Cell Signaling, 2F9, 4856, 1:2000), anti-S6 ribosomal protein (rabbit polyclonal, Cell Signaling, 5G10, 2217, 1:2000). Secondary antibodies used included: anti-rabbit HRP antibody (31460, Thermo Scientific Pierce Antibodies, 1:10,000), anti-rabbit Alexa 488 (A-A11070, Invitrogen, 1:1000), anti-mouse Alexa 555 (A-21425, Invitrogen, 1:1000) and anti-chick 488 (A11039, Invitrogen, 1:1000).

Image analysis and quantification

Confocal images (×40 field) were acquired on a SPE confocal microscope (Leica). Images were reconstructed using *z*-stack projection using FIJI software. FISH signal quantification was performed on raw images by manually delimiting nucleoli, nucleus, whole cell or whole myofibres as individual regions of interest (ROI). The fluorescence intensity provided by FIJI corresponds to raw integrative density for each ROI. Cross-sectional areas were defined using FIJI on TIFF images of anti-laminin immunostained cryosections. Images of cell staining of p-RPS6 were performed on Zeiss Observer microscopes. The fluorescence intensity provided by FIJI corresponds to the integrative density for each ROI. Approximately 100 cells were quantified for each time point; *n*-values are specified for each experiment in the figure legends or figures.

Live imaging

Cells isolated by FACS were plated on Matrigel-coated 24-well glass-bottom plates (P24G-0-10F; MatTek Corporation) with growth medium. The plate was then incubated for 20 h at 37°C, 5% CO_2, and 3% O_2 (Zeiss). Cells were then imaged up to 30 h with a Zeiss AxioObserver Z1 with an LCI PlnN 10×0.8 W DICII objective and AxioCam camera. An area of interest was cropped, and four to eight representative cells were tracked manually using TrackMate on FIJI.

Statistics analysis

For comparison between two groups, the two-tailed Student's *t*-test was performed to calculate *P* values and to determine statistically significant differences (*P<0.05; **P<0.01; ***P<0.001). Between three and five mice were analysed for most experiments. Data are presented as mean±s.d.

Acknowledgements

We thank Patricia Flamant and Clémire Cimper for the histology and cryosections and Jean-Yves Tinevez at the Imaging Platform for assistance with cell tracking. We also thank Sophie Novault (Flow Cytometry Platform of the Technology Core at the Center for Translational Science at Institut Pasteur).

Competing interests

The authors declare no competing or financial interests.

Author contributions

Conceptualization: B.G.-M., S.T.; Methodology: B.G.-M., M.C.-T., S.T.; Validation: B.G.-M.; Formal analysis: B.G.-M.; Investigation: B.G.-M., M.C.-T., S.T.; Resources: M.L.B., P.-H.C., M.C.-T., S.T.; Data curation: B.G.-M.; Writing - original draft: B.G.-M., S.T.; Writing - review & editing: B.G.-M., M.C.-T., S.T.; Visualization: B.G.-M.; Supervision: M.C.-T., S.T.; Project administration: S.T.; Funding acquisition: S.T.

Funding
S.T. and M.C.-T. acknowledge support from the Institut Pasteur and the Agence Nationale de la Recherche (Laboratoire d'Excellence Revive, Investissement d'Avenir; ANR-10-LABX-73).

Supplementary information
Supplementary information available online at
http://dev.biologists.org/lookup/doi/10.1242/dev.162636.supplemental

References

Agrawal, M. G. and Bowman, L. H. (1987). Transcriptional and translational regulation of ribosomal protein formation during mouse myoblast differentiation. *J. Biol. Chem.* **262**, 4868-4875.
Armistead, J. and Triggs-Raine, B. (2014). Diverse diseases from a ubiquitous process: the ribosomopathy paradox. *FEBS Lett.* **588**, 1491-1500.
Baßler, J., Paternoga, H., Holdermann, I., Thoms, M., Granneman, S., Barrio-Garcia, C., Nyarko, A., Lee, W., Stier, G., Clark, S. A. et al. (2014). A network of assembly factors is involved in remodeling rRNA elements during preribosome maturation. *J. Cell Biol.* **207**, 481-498.
Buszczak, M., Signer, R. A. J. and Morrison, S. J. (2014). Cellular differences in protein synthesis regulate tissue homeostasis. *Cell* **159**, 242-251.
Chaillou, T., Kirby, T. J. and McCarthy, J. J. (2014). Ribosome biogenesis: emerging evidence for a central role in the regulation of skeletal muscle mass. *J. Cell. Physiol.* **229**, 1584-1594.
Chakkalakal, J. V., Jones, K. M., Basson, M. A. and Brack, A. S. (2012). The aged niche disrupts muscle stem cell quiescence. *Nature* **490**, 355-360.
Cormier, S., Le Bras, S., Souilhol, C., Vandormael-Pournin, S., Durand, B., Babinet, C., Baldacci, P. and Cohen-Tannoudji, M. (2006). The murine ortholog of notchless, a direct regulator of the notch pathway in Drosophila melanogaster, is essential for survival of inner cell mass cells. *Mol. Cell. Biol.* **26**, 3541-3549.
de la Cruz, J., Sanz-Martinez, E. and Remacha, M. (2005). The essential WD-repeat protein Rsa4p is required for rRNA processing and intra-nuclear transport of 60S ribosomal subunits. *Nucleic Acids Res.* **33**, 5728-5739.
Fromont-Racine, M., Senger, B., Saveanu, C. and Fasiolo, F. (2003). Ribosome assembly in eukaryotes. *Gene* **313**, 17-42.
Gayraud-Morel, B., Chrétien, F., Flamant, P., Gomès, D., Zammit, P. S. and Tajbakhsh, S. (2007). A role for the myogenic determination gene Myf5 in adult regenerative myogenesis. *Dev. Biol.* **312**, 13-28.
Gayraud-Morel, B., Chretien, F., Jory, A., Sambasivan, R., Negroni, E., Flamant, P., Soubigou, G., Coppee, J.-Y., Di Santo, J., Cumano, A. et al. (2012). Myf5 haploinsufficiency reveals distinct cell fate potentials for adult skeletal muscle stem cells. *J. Cell Sci.* **125**, 1738-1749.
Gayraud-Morel, B., Pala, F., Sakai, H. and Tajbakhsh, S. (2017). Isolation of muscle stem cells from mouse skeletal muscle. *Methods Mol. Biol.* **1556**, 23-39.
Golomb, L., Volarevic, S. and Oren, M. (2014). p53 and ribosome biogenesis stress: the essentials. *FEBS Lett.* **588**, 2571-2579.
Gray, J. V., Petsko, G. A., Johnston, G. C., Ringe, D., Singer, R. A. and Werner-Washburne, M. (2004). "Sleeping beauty": quiescence in Saccharomyces cerevisiae. *Microbiol. Mol. Biol. Rev.* **68**, 187-206.
Hardy, D., Besnard, A., Latil, M., Jouvion, G., Briand, D., Thépenier, C., Pascal, Q., Guguin, A., Gayraud-Morel, B., Cavaillon, J.-M. et al. (2016). Comparative study of injury models for studying muscle regeneration in mice. *PLoS ONE* **11**, e0147198.
Jacobs, F. A., Bird, R. C. and Sells, B. H. (1985). Differentiation of rat myoblasts. Regulation of turnover of ribosomal proteins and their mRNAs. *Eur. J. Biochem.* **150**, 255-263.
Keefe, A. C., Lawson, J. A., Flygare, S. D., Fox, Z. D., Colasanto, M. P., Mathew, S. J., Yandell, M. and Kardon, G. (2015). Muscle stem cells contribute to myofibres in sedentary adult mice. *Nat. Commun.* **6**, 7087.
Kondrashov, N., Pusic, A., Stumpf, C. R., Shimizu, K., Hsieh, A. C., Xue, S., Ishijima, J., Shiroishi, T. and Barna, M. (2011). Ribosome-mediated specificity in Hox mRNA translation and vertebrate tissue patterning. *Cell* **145**, 383-397.
Lang, F., Aravamudhan, S., Nolte, H., Türk, C., Hölper, S., Müller, S., Günther, S., Blaauw, B., Braun, T. and Krüger, M. (2017). Dynamic changes in the mouse skeletal muscle proteome during denervation-induced atrophy. *Dis. Model Mech.* **10**, 881-896.
Le Bouteiller, M., Souilhol, C., Beck-Cormier, S., Stedman, A., Burlen-Defranoux, O., Vandormael-Pournin, S., Bernex, F., Cumano, A. and Cohen-Tannoudji, M. (2013). Notchless-dependent ribosome synthesis is required for the maintenance of adult hematopoietic stem cells. *J. Exp. Med.* **210**, 2351-2369.
Lindstrom, M. S. (2009). Emerging functions of ribosomal proteins in gene-specific transcription and translation. *Biochem. Biophys. Res. Commun.* **379**, 167-170.
Livak, K. J. and Schmittgen, T. D. (2001). Analysis of relative gene expression data using real-time quantitative PCR and the 2(-Delta Delta C(T)) Method. *Methods* **25**, 402-408.
Matsuo, Y., Granneman, S., Thoms, M., Manikas, R.-G., Tollervey, D. and Hurt, E. (2014). Coupled GTPase and remodelling ATPase activities form a checkpoint for ribosome export. *Nature* **505**, 112-116.
Mills, E. W. and Green, R. (2017). Ribosomopathies: there's strength in numbers. *Science* **358**, eaan2755.
Miniou, P., Tiziano, D., Frugier, T., Roblot, N., Le Meur, M. and Melki, J. (1999). Gene targeting restricted to mouse striated muscle lineage. *Nucleic Acids Res.* **27**, e27-e30.
Mourikis, P., Sambasivan, R., Castel, D., Rocheteau, P., Bizzarro, V. and Tajbakhsh, S. (2012). A critical requirement for notch signaling in maintenance of the quiescent skeletal muscle stem cell state. *Stem Cells* **30**, 243-252.
Nerurkar, P., Altvater, M., Gerhardy, S., Schütz, S., Fischer, U., Weirich, C. and Panse, V. G. (2015). Eukaryotic ribosome assembly and nuclear export. *Int. Rev. Cell Mol. Biol.* **319**, 107-140.
Norton, L. E. and Layman, D. K. (2006). Leucine regulates translation initiation of protein synthesis in skeletal muscle after exercise. *J. Nutr.* **136**, 533S-537S.
O'Donohue, M.-F., Choesmel, V., Faubladier, M., Fichant, G. and Gleizes, P.-E. (2010). Functional dichotomy of ribosomal proteins during the synthesis of mammalian 40S ribosomal subunits. *J. Cell Biol.* **190**, 853-866.
Pawlikowski, B., Pulliam, C., Betta, N. D., Kardon, G. and Olwin, B. B. (2015). Pervasive satellite cell contribution to uninjured adult muscle fibers. *Skelet. Muscle* **5**, 42.
Pechmann, S., Willmund, F. and Frydman, J. (2013). The ribosome as a hub for protein quality control. *Mol. Cell* **49**, 411-421.
Peña, C., Hurt, E. and Panse, V. G. (2017). Eukaryotic ribosome assembly, transport and quality control. *Nat. Struct. Mol. Biol.* **24**, 689-699.
Relaix, F. and Zammit, P. S. (2012). Satellite cells are essential for skeletal muscle regeneration: the cell on the edge returns centre stage. *Development* **139**, 2845-2856.
Rocheteau, P., Gayraud-Morel, B., Siegl-Cachedenier, I., Blasco, M. A. and Tajbakhsh, S. (2012). A subpopulation of adult skeletal muscle stem cells retains all template DNA strands after cell division. *Cell* **148**, 112-125.
Ross, A. P. and Zarbalis, K. S. (2014). The emerging roles of ribosome biogenesis in craniofacial development. *Front Physiol.* **5**, 26.
Sambasivan, R., Gayraud-Morel, B., Dumas, G., Cimper, C., Paisant, S., Kelly, R. G. and Tajbakhsh, S. (2009). Distinct regulatory cascades govern extraocular and pharyngeal arch muscle progenitor cell fates. *Dev. Cell* **16**, 810-821.
Seale, P., Sabourin, L. A., Girgis-Gabardo, A., Mansouri, A., Gruss, P. and Rudnicki, M. A. (2000). Pax7 is required for the specification of myogenic satellite cells. *Cell* **102**, 777-786.
Siegel, A. L., Kuhlmann, P. K. and Cornelison, D. D. W. (2011). Muscle satellite cell proliferation and association: new insights from myofiber time-lapse imaging. *Skelet. Muscle* **1**, 7.
Signer, R. A., Magee, J. A., Salic, A. and Morrison, S. J. (2014). Haematopoietic stem cells require a highly regulated protein synthesis rate. *Nature* **509**, 49-54.
Signer, R. A. J., Qi, L., Zhao, Z., Thompson, D., Sigova, A. A., Fan, Z. P., DeMartino, G. N., Young, R. A., Sonenberg, N. and Morrison, S. J. (2016). The rate of protein synthesis in hematopoietic stem cells is limited partly by 4E-BPs. *Genes Dev.* **30**, 1698-1703.
Stec, M. J., Mayhew, D. L. and Bamman, M. M. (2015). The effects of age and resistance loading on skeletal muscle ribosome biogenesis. *J. Appl. Physiol. (1985)* **119**, 851-857.
Stedman, A., Beck-Cormier, S., Le Bouteiller, M., Raveux, A., Vandormael-Pournin, S., Coqueran, S., Lejour, V., Jarzebowski, L., Toledo, F., Robine, S. et al. (2015). Ribosome biogenesis dysfunction leads to p53-mediated apoptosis and goblet cell differentiation of mouse intestinal stem/progenitor cells. *Cell Death Differ.* **22**, 1865-1876.
Xue, S. and Barna, M. (2012). Specialized ribosomes: a new frontier in gene regulation and organismal biology. *Nat. Rev. Mol. Cell Biol.* **13**, 355-369.
Xue, S., Tian, S., Fujii, K., Kladwang, W., Das, R. and Barna, M. (2015). RNA regulons in Hox 5′ UTRs confer ribosome specificity to gene regulation. *Nature* **517**, 33-38.
Zammit, P. S. and Beauchamp, J. R. (2001). The skeletal muscle satellite cell: stem cell or son of stem cell? *Differentiation* **68**, 193-204.
Zhang, Y., Wolf, G. W., Bhat, K., Jin, A., Allio, T., Burkhart, W. A. and Xiong, Y. (2003). Ribosomal protein L11 negatively regulates oncoprotein MDM2 and mediates a p53-dependent ribosomal-stress checkpoint pathway. *Mol. Cell. Biol.* **23**, 8902-8912.
Zhang, Q., Shalaby, N. A. and Buszczak, M. (2014). Changes in rRNA transcription influence proliferation and cell fate within a stem cell lineage. *Science* **343**, 298-301.
Zhou, X., Liao, W.-J., Liao, J.-M., Liao, P. and Lu, H. (2015). Ribosomal proteins: functions beyond the ribosome. *J. Mol. Cell Biol.* **7**, 92-104.
Zismanov, V., Chichkov, V., Colangelo, V., Jamet, S., Wang, S., Syme, A., Koromilas, A. E. and Crist, C. (2016). Phosphorylation of eIF2alpha is a translational control mechanism regulating muscle stem cell quiescence and self-renewal. *Cell Stem Cell* **18**, 79-90.

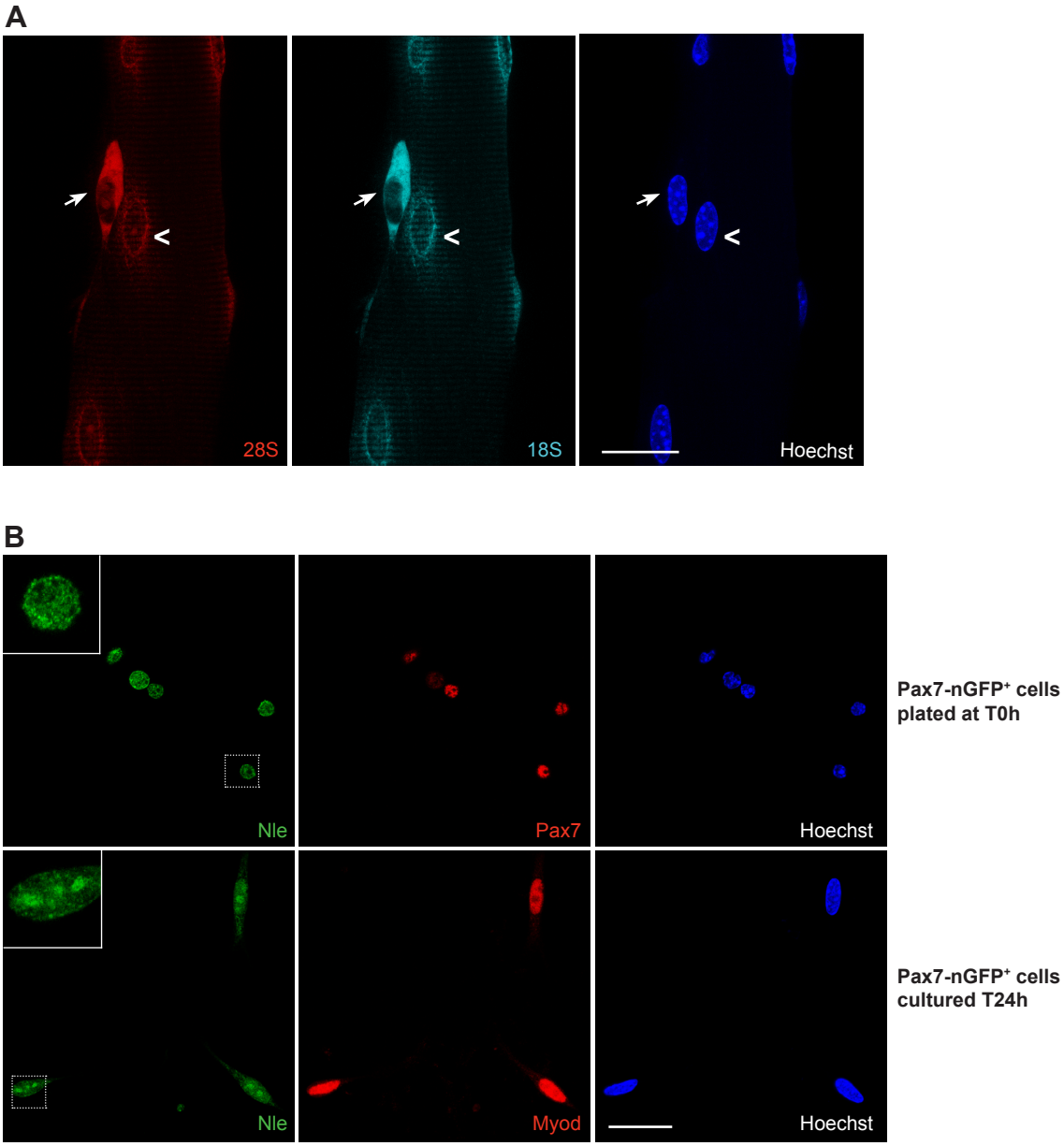

Figure S1. Nle protein and ribosomal RNA expression during myogenesis.

A) Representative images of rRNA FISH on cultured (T24h) *Tg:Pax7-nGFP* myofibres. Note high levels of total 18S and 28S in activated satellite cells (arrows); rRNAs indicate ribosomes located throughout myofibre, and enriched around myonuclei (arrowhead).

B) Representative images of Nle immunostaining on T0h and 24h cultured satellite cells, co-stained with Pax7 and Myod respectively. Note Nle nucleolar staining in activated satellite cells, and faint staining in nuclei of quiescent cells. Scale bar A and B, 20μm.

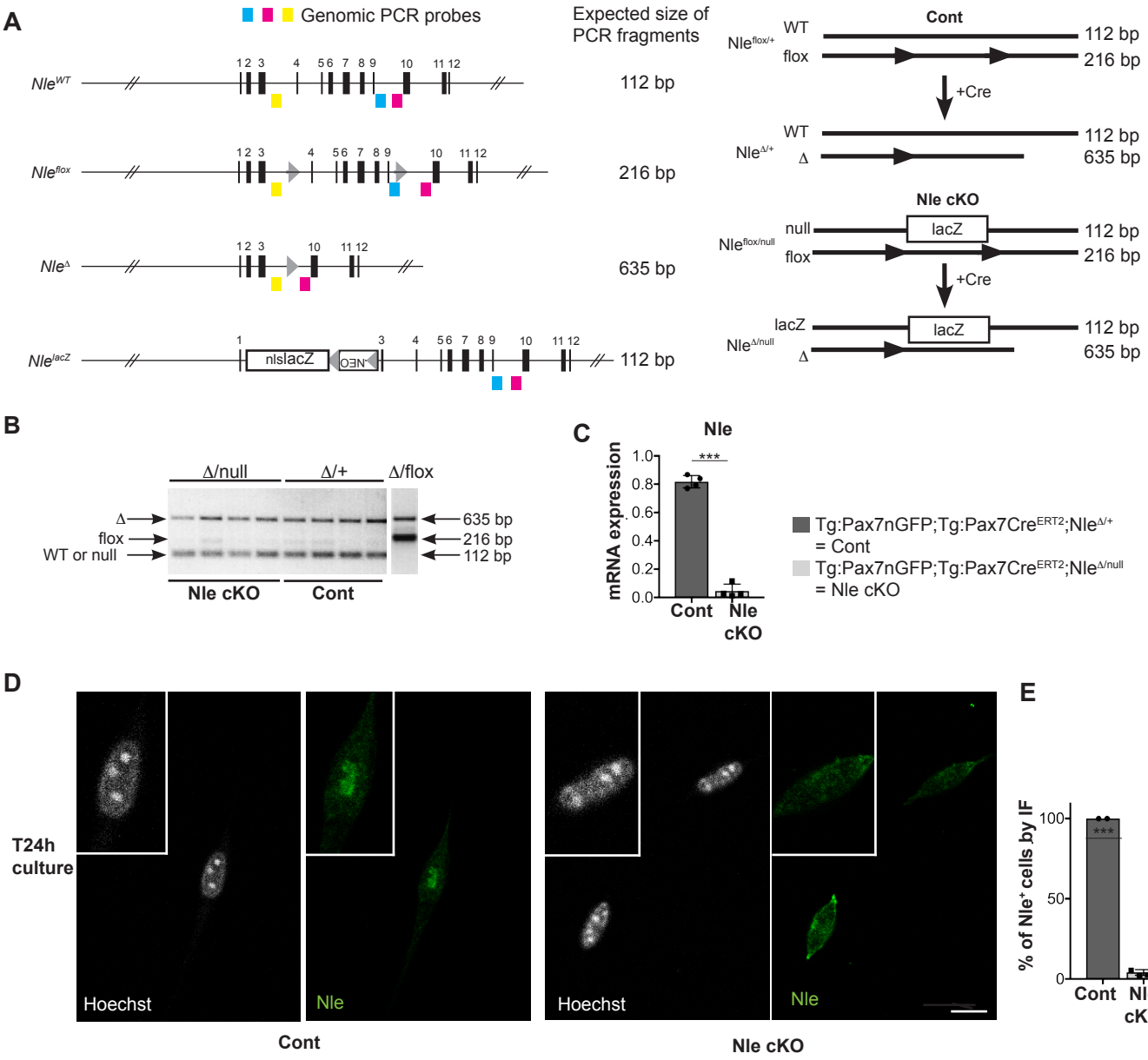

Figure S2. *Nle* deficiency in satellite cells.

A) Scheme of WT and recombined *Nle* alleles. Upon tamoxifen treatment and nuclear expression of *Cre* recombinase, control and mutant mice recombined the floxed allele deleting exons 4-9(Δ), generating a non-functional allele. WT and null (*lacZ*) alleles are indicated.

B) Genomic PCR for *Nle* deletion on isolated satellite cells. After tamoxifen treatment, the floxed allele was efficiently recombined in quiescent satellite cells. Far right lane (Δ/flox), internal PCR control detecting the floxed and deleted alleles (Le Bouteiller et al., 2013).

C) *Nle* expression in control and mutant quiescent satellite cells; reduction of 95% of *Nle* transcripts after *Cre*-recombination.

D) Immunofluorescence of Nle protein in 24h cultured satellite cells. Note nuclear staining in control-activated cells, but not in mutant cells.

E) Quantification of Nle^{+} cells by immunofluorescence at 24h on cells cultured *in vitro*.

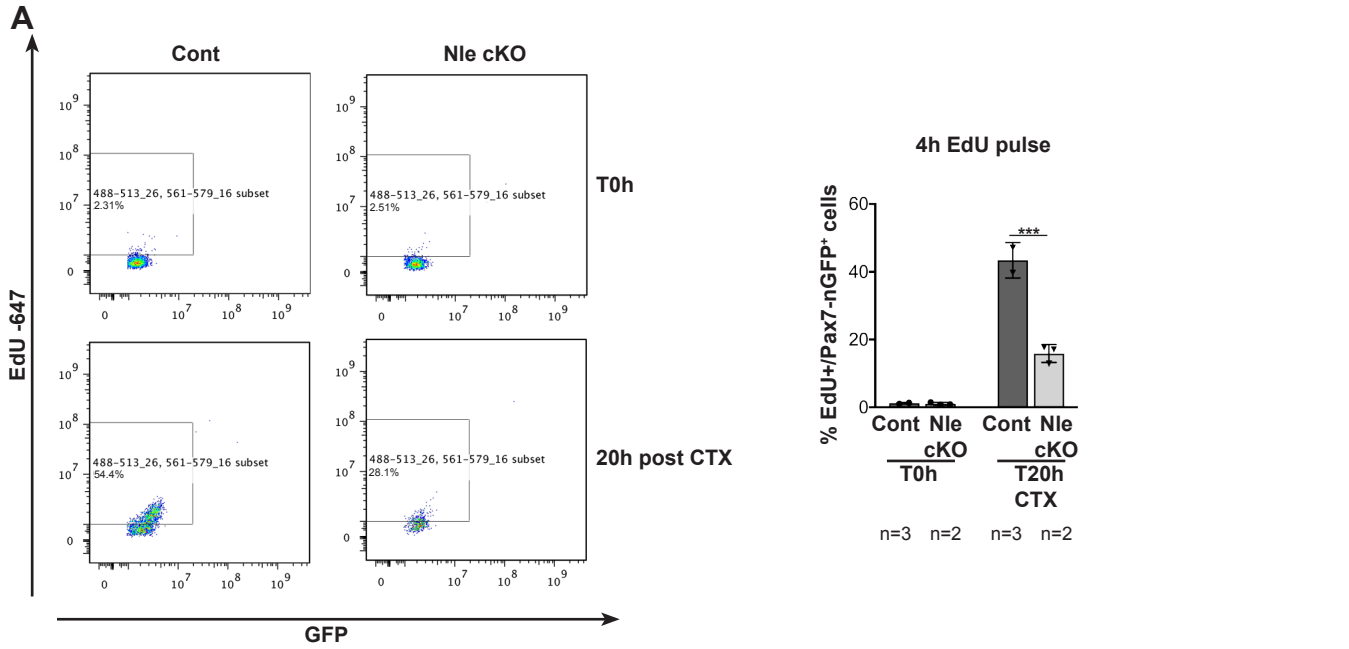

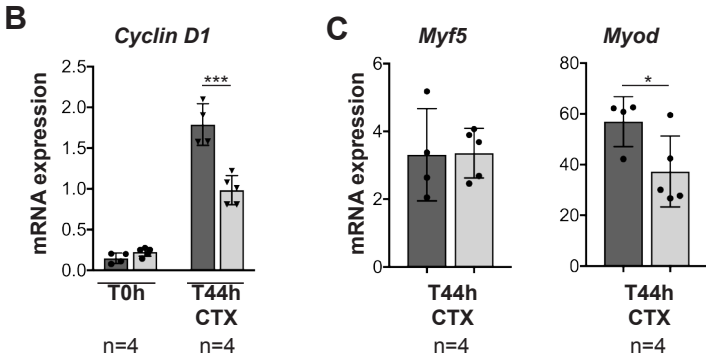

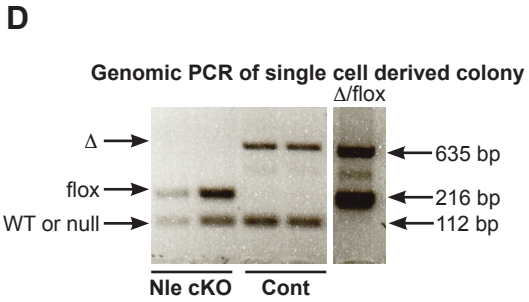

Tg:Pax7nGFP;Tg:Pax7Cre^{ERT2};Nle$^{\Delta/+}$
= Cont

Tg:Pax7nGFP;Tg:Pax7Cre^{ERT2};Nle$^{\Delta/null}$
= Nle cKO

Figure S3. Failure of proliferation of *Nle* cKO satellite cells.

A) FACS profiles of *in vitro* EdU labeling of control and mutant injury-activated satellite cells with 4h EdU pulse of TA muscles collected 20h after CTX injury. Upper leg muscles were used to isolate control quiescent cells; 20h after CTX injury, mutant cells showed a lower number of EdU-labeled cells.

B, C) RT-qPCR of markers for cell cycle (*Cyclin D1*) and myogenic regulatory factors *Myod*, *Myf5*, in control and *Nle*-deleted satellite cells.

D) Genomic PCR single cell cloning colonies after 3 weeks in culture; note rare single cell derived colonies in *Nle* cKO cultures contained only the undeleted Nle^{flox} allele (flox) and the null allele, indicating that these cells are escapers (did not recombine the floxed allele); single cell-derived colonies from control muscles showed WT and recombined floxed allele (Δ).

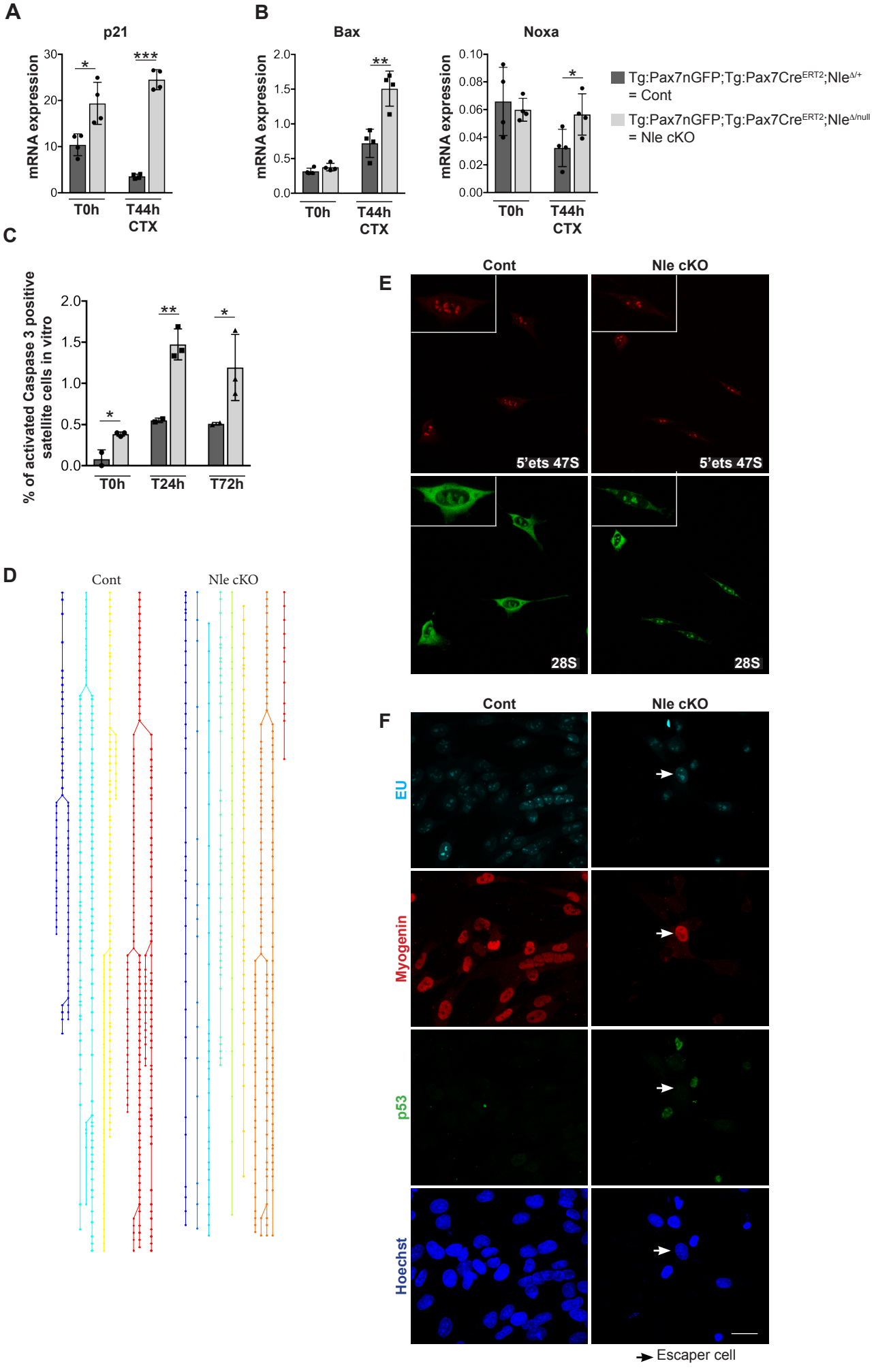

Figure S4. Apoptosis and nucleolar integrity of Nle cKO cells.

A) Quantification by RT-qPCR of *p21* mRNA expression in quiescent and cardiotoxin-activated Cont and Nle cKO cells.

B) Quantification by RT-qPCR of apoptotic genes *Bax* and *Noxa* mRNA expression in quiescent and cardiotoxin-activated Cont and *Nle* cKO cells.

C) Percentage of activated-Caspase 3 positive satellite cells at T0h, T24h and T72h after in vitro culture.

D) Cell tracking overview of Cont (Movie 1) and *Nle* cKO (Movie 2) cells. Note that Cont cells divide several times and most *Nle* cKO cells do not divide. Among *Nle* cKO cells, one cell is undergoing cell division and corresponds likely to a non-recombined escaper cell.

E) Representative images of rRNA FISH in cultured Cont and *Nle* cKO cells at T24h. The 5'ets probe hybridized only unprocessed 47S rRNA located in nucleoli. The 28S probe localized rRNAs in all cellular compartments. Both show a similar well defined nucleoli in Cont and *Nle* cKO cells.

F) Representative staining of 5-Ethynyl–Uridine (EU) staining of cells cultured for 4 days. Both Cont and *Nle* cKO cells show a nucleolar staining for newly generated rRNAs after 4h pulse with EU. After 4d in culture, only Cont cells expressed the differentiation marker Myogenin, while *Nle* cKO cells are positives for p53. Arrow indicates an escaper cell, positive for Myogenin and negative for p53.

For RT-qPCR 3-4 mice were used for each time point; TBP was used as reference gene. Scale bar, 20μm

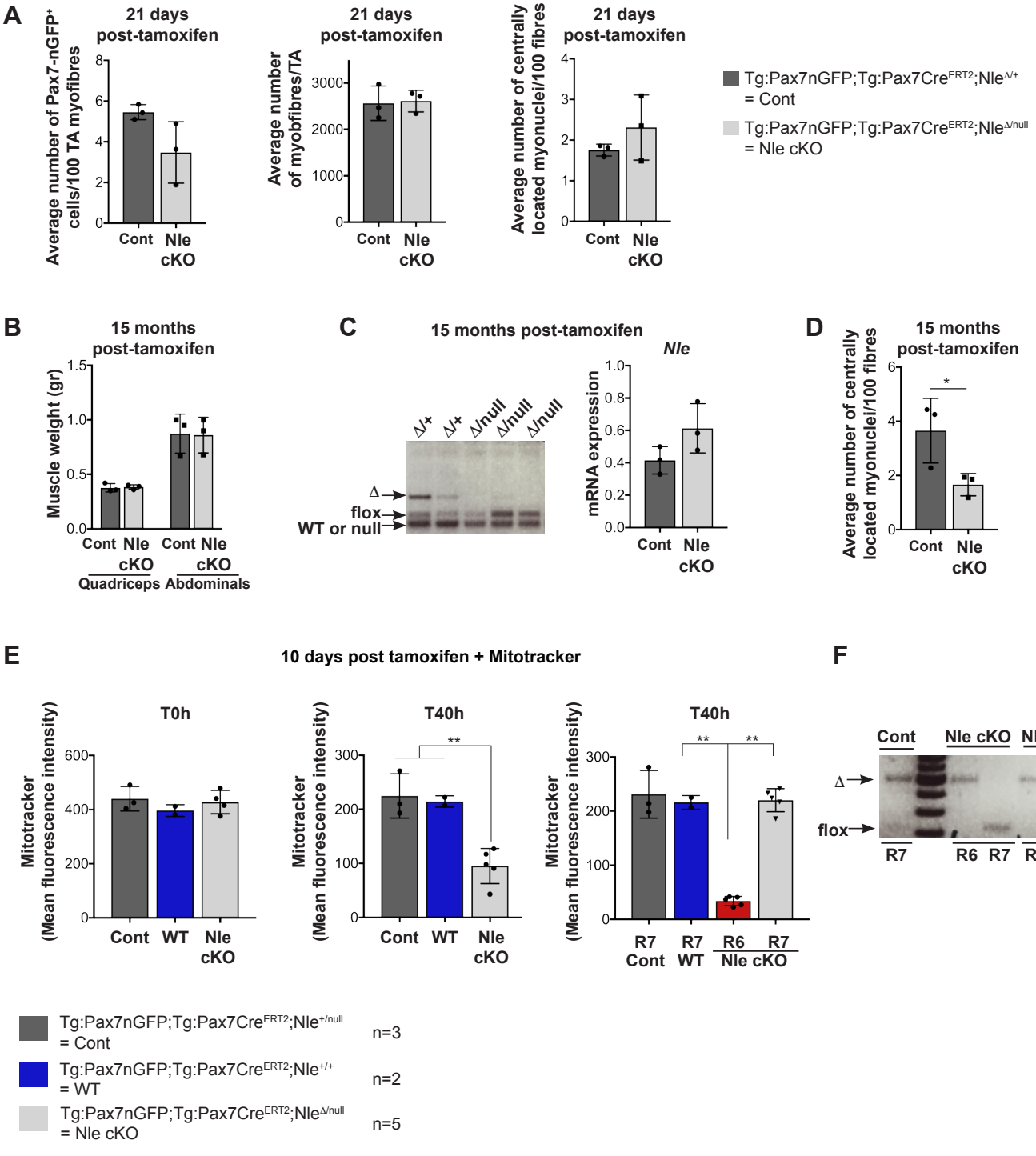

Figure S5. Long-term loss of *Nle* cKO satellite cells during homeostasis.

A) Analysis of satellite cells and myofibres 21 days post-tamoxifen treatment.

B) Quadriceps and abdominal muscle weight 15-months post-tamoxifen treatment.

C) Representative genomic PCR of isolated Pax7-nGFP+ satellite cells from 15-month post-tamoxifen treated muscles. Only the non-recombined allele was found 15-months post-tamoxifen treatment, indicating the prevalence of escaper cells after a long period in homeostatic muscles. Expression of *Nle* mRNA 15-months post-tamoxifen treatment (right graph).

D) Average number of centrally located myonuclei/100 TA myofibres from Cont and *Nle* cKO 15 months old mice. n=3 mice, around 2000 myofibres on 2 different sections were counted.

E) Mitochondria quantification on WT, heterozygous and mutant cells. The number of mitochondria was unchanged in controls (WT and flox/+) and mutant (Null/Δ) cells in quiescence but the number of mitochondria decreased dramatically in the *Nle* mutant (flox/Δ) cells (Red R6).

F) Genomic PCR of floxed and deleted (Δ) alleles of cells isolated by FACS after mitotrackerT staining. Only the R7 population was observed in Cont cells, showing the deleted allele (Δ/+). In *Nle* cKO cells, both R6 and R7 were observed. The R6 population had a low mitochondrial content, showed the deleted (Δ) allele, and corresponded to the (*Nle* null cells), whereas R7 represents a minor population with a mitochondrial content equivalent to control and showed the floxed allele corresponding to escaper cells.

Movie 1. Time lapse imaging of Nle cKO cells in culture after isolation by FACS.

Movie 2. Time lapse imaging of control satellite cells in culture after isolation by FACS.

Table S1. Sequences of RT-qPCR primers

Target gene	Forward primer	Reverse primer
Nle	TCCTTAGCATATCCTGGTCCC	GCACTCGGGGTTCATGTGA
its1	TCTGACCTCGCCACCCTA	CCTCGTAGACACGGAAGAGC
Its2	TGTGTGTGTTTGGGTCTTGC	GGATACCACCTCTCTCCGTTC
18S	CGGCTACCACACATCCAAGGAA	GCTGGAATTACCGCGGCT
28S	TCATCAGACCCCAGAAAAGG	GATTCGGCAGGTGAGTTGTT
CyclinE	CAGTCCGCTCCAGAAAAAGG	GGTCCACGCATGCTGAATTA
CyclinD1	CACACGGACTACAGGGGAG	CACAGGAGCTGGTGTTCCAT
TroponinT	CCTCATTGACAGCCACTTTG	TCTCAGCGCAATTCTTTG
p21	CCCTCTATTTTGGAGGGTTAATCT	GTACCCTGCATATACATTCCCTTC
Bax	GCCGGAGCTACCTGTTTTTAG	GACAAAGCCACACATGACCAG
Noxa	GCAGAGCTACCACCTGAGTTC	CTTTTGCGACTTCCCAGGCA
TBP	AGAACAATCCAGACTAGCAGC	GGGAACTTCACATCACAGCTC

Target gene	Taqman primer
Myogenin	Mm00446195_g1
Myod	Mm01203489_g1
Myf5	Mm00435125_m1
HeyL	Mm00516555_m1
TBP	Mm00446971_m1

Key resources

Antibody	Reference	Dilution
Anti GFP, Chicken polyclonal	Abcam, ab13970	1:1000
Anti-Laminin, Rabbit polyclonal	Sigma, L9393	1:400
Anti-Myogenin, Mouse monoclonal	DSHB, F5D	1:50
Anti-Pax7, Mouse monoclonal	DHSB, Pax7	1:50
Anti-Myod, Mouse monoclonal	Dako, Clone 5.8A, M3512	1:100
Anti-phospho-S6 RP, Rabbit polyclonal	Cell Signaling, 2F9, 4856	1:2000
Anti-S6 RP, Rabbit polyclonal	Cell Signaling, 5G10, 2217	1:2000
Anti-Notchless, Rabbit Polyclonal	(Le Bouteiller et al., 2013)	1:100

Mice	References
Tg:Pax7-nGFP	(Sambasivan et al., 2009)
Tg:Pax7-Cre^{ERT2}	(Mourikis et al., 2012)
Nle$^{flox/null}$	(Cormier et al., 2006)
Tg:HSA-Cre	(Miniou et al., 1999)